ELSEVIER

Journal of Structural Geology 30 (2008) 138–158

JOURNAL OF STRUCTURAL GEOLOGY

www.elsevier.com/locate/jsg

Significance of transport-parallel strain variations in part of the Raft River shear zone, Raft River Mountains, Utah, USA

W.A. Sullivan*

Department of Geology, Colby College, 5800 Mayflower Hill, Waterville, ME 04901, USA

Received 21 July 2007; received in revised form 10 November 2007; accepted 21 November 2007
Available online 28 November 2007

Abstract

This paper examines part of the Raft River shear zone (RRSZ) in northwestern Utah that exhibits an extreme transport-parallel increase in strain intensity coupled with a transition from flattening to constrictional strain. Detailed geologic mapping and finite-strain, quartz-*c*-axis-fabric, and kinematic-vorticity analyses demonstrate local necking of the shear zone associated with an increase in transport-parallel elongation accommodated by a stretching fault at the base of the shear zone. The domain of intense deformation and necking of the shear zone is localized where the basal stretching fault cuts rheologically weak rocks. This domain is characterized by strain in the constrictional field caused by transport-perpendicular flow into the area of high transport-parallel elongation. Where rocks cut by the stretching fault are rheologically strong, the RRSZ locally records flattening strain and lower strain intensities, limiting the amount of stretching needed at the base of the shear zone in any one direction and/or recording transport-perpendicular flow into adjacent highly extended domains. The rheology of rocks cut by the stretching fault directly controlled the amount and style of zone-normal shortening and transport-parallel elongation, and these observations provide an example of deformation partitioning in a crustal-scale structure driven by local rheological transitions.
© 2007 Elsevier Ltd. All rights reserved.

Keywords: Constrictional strain; Rheology; Strain-path partitioning; Raft River shear zone; Raft River Mountains; Strain partitioning; Finite-strain variations

1. Introduction

Plastic high-strain zones have traditionally been interpreted in terms of two-dimensional, homogeneous deformation (e.g., plane strain). However, analyses of naturally deformed rocks show us that deviations from plane strain and two-dimensional flow not only exist but are common in nature (Pfiffner and Ramsay, 1982, their Fig. A1). Such variations in the shape of the finite-strain ellipsoid, or strain geometry, occur in contractional, extensional, transcurrent, transpressional, and transtensional tectonic regimes (e.g., Twiss and Moores, 1992; Moores and Twiss, 1995; Holdsworth et al., 1998; Dewey, 2002). Deviation from plane strain has also been recorded in a wide variety of local structural settings such as fold hinge-zones and limbs (e.g., Law, 1986; Holst and Fossen, 1987; Sullivan, 2006); the margins of forcefully emplaced plutons (e.g., Compton, 1955); metamorphic soles beneath ophiolitic allochthons (Flinn, 1992; Hacker and Mosenfelder, 1996); and extensional, contractional, transcurrent, transpressional, and transtensional plastic shear zones (e.g., Hossack, 1968; Fletcher and Bartley, 1994; Lin and Jiang, 2001; Dewey, 2002; Czeck and Hudleston, 2003; Strine and Wojtal, 2004; Giorgis and Tikoff, 2004). Such deviations in strain geometry are also commonly associated with significant variations in the amount of finite strain, or strain intensity, which occur in a seemingly non-systematic way. In shear zones that have traditionally been interpreted as relatively straight-sided, planar features variations in strain geometry and along-transport variations in strain intensity should lead to strain compatibility problems (Ramsay and Graham, 1970; Hudleston, 1999), and, at the very least, these variations can significantly complicate traditional two-dimensional kinematic analyses (Tikoff and Greene, 1997; Jones et al., 2004; Bailey et al., 2004). It is likely that these deviations from plane strain and variations

* Tel.: +1 207 859 5803.
E-mail address: wasulliv@colby.edu

0191-8141/$ - see front matter © 2007 Elsevier Ltd. All rights reserved.
doi:10.1016/j.jsg.2007.11.007

in strain intensity are providing us with significant information about the way strain is accommodated in the middle and lower crust. Until recently, however, such finite-strain variations in natural high-strain zones were commonly overlooked in the literature. This is especially true for constrictional strains (Solar and Valentino, 2003). Indeed, we still have little information about how finite-strain variations are linked to such factors as internal variations in rheology and kinematic vorticity and variations in the external geometry and boundary conditions imposed on high-strain zones.

To address this gap in our understanding of strain partitioning in plastic high-strain zones, I present a detailed case study of part of a footwall shear zone of a metamorphic core complex, the Raft River shear zone (RRSZ), in the Raft River Mountains of northwestern Utah. This locality was first documented by Wells (2001), and it exhibits a wide range of measured finite-strain intensities and strain geometries including a large domain of strain in the constrictional field. In this paper I argue that these strain heterogeneities are directly controlled by along-transport variations in the rheology of rocks that are cut by a stretching fault (Means, 1989) at the lower boundary of the shear zone that accommodates zone-normal shortening and transport-parallel elongation. The results of this study provide a better understanding of how and why strain is partitioned in plastic high-strain zones and will ultimately help geoscientists encountering such strain variations to better interpret them. Moreover, because the RRSZ is a footwall shear zone of a metamorphic core complex (Malavieille, 1987a; Wells et al., 2000), a fundamental crustal structure (Wernicke and Axen, 1988; Whitney et al., 2004), these results also provide a better understanding of how these crustal-scale structures evolve and control the partitioning of strain in extensional tectonic settings.

2. Regional geologic setting

The Raft River Mountains comprise the easternmost segment of a large Cordilleran metamorphic core complex, the Albion–Raft River–Grouse Creek metamorphic core complex, that includes the Albion Mountains, Raft River Mountains, and Grouse Creek Mountains in northwestern Utah and southern Idaho, USA (Fig. 1) (Armstrong, 1968; Compton, 1972, 1975; Compton et al., 1977; Coney, 1980; Snoke and Miller, 1988; Sullivan and Snoke, 2007). The lowest structural levels of the core complex expose the Green Creek complex of Armstrong (1968) that includes Late Archean adamellite and adamellite orthogneiss that intrude metatrondhjemite, metagabbro, hornblende schist, and biotite schist (Armstrong, 1968; Compton et al., 1977; Todd, 1980; Miller, 1980). In the Raft River Mountains the Archean rocks are nonconformably overlain by the Proterozoic Elba Quartzite and the overlying schist member of the Elba Quartzite, and the core complex

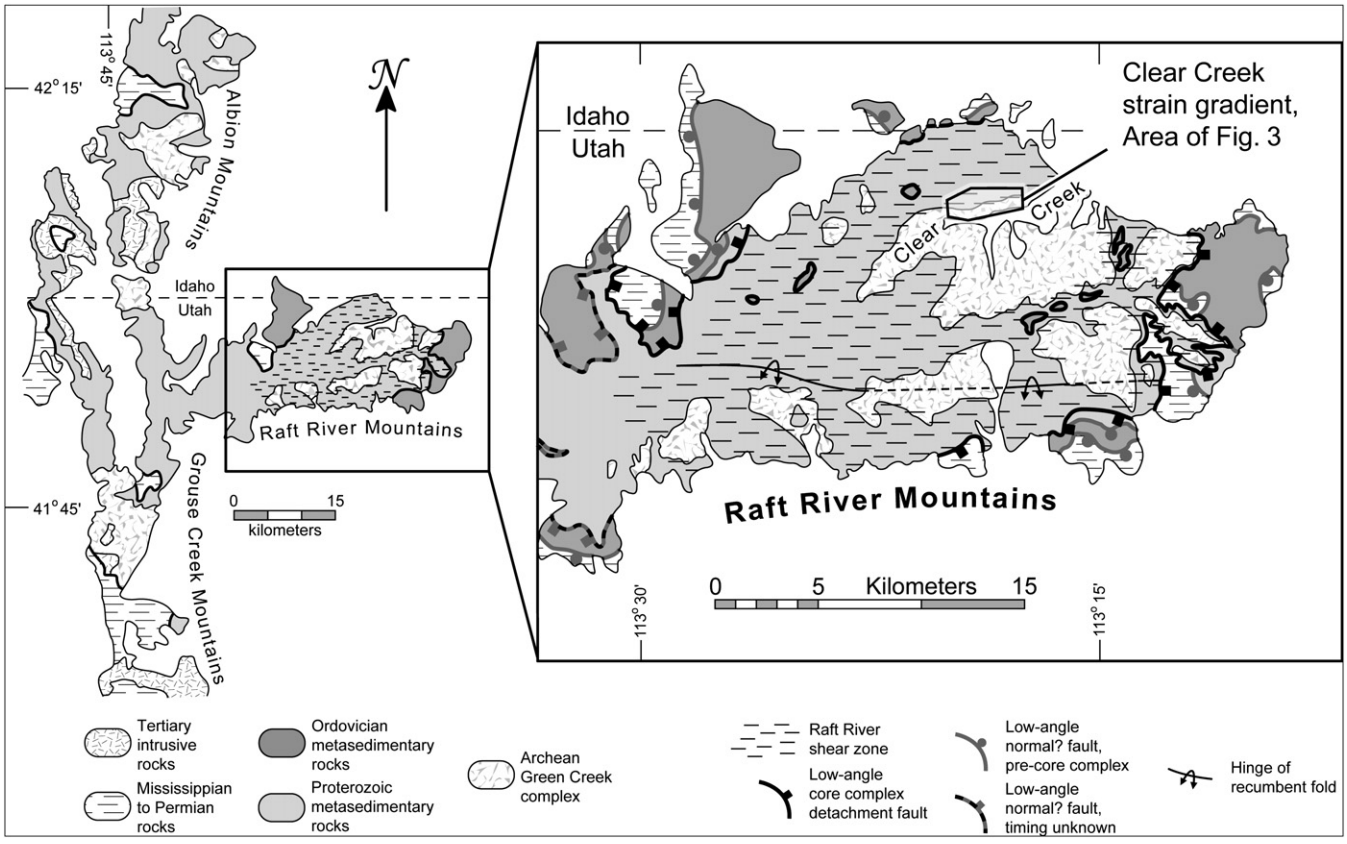

Fig. 1. Simplified geologic map of the Albion–Raft River–Grouse Creek metamorphic core complex and a more detailed geologic map of the Raft River Mountains showing major structures, intrusive bodies, and the location of Fig. 3. Adapted and compiled from Wells, (1997, 2001); Miller (1980); Compton et al. (1977), and Compton (1972, 1975).

is bounded by the low-angle RRSZ and associated frictional/brittle Raft River detachment fault (Compton, 1972, 1975; Compton et al., 1977; Malavieille, 1987a; Wells, 2001). $^{40}Ar/^{39}Ar$ cooling ages of muscovite from the RRSZ range from 47 Ma in the westernmost parts of the range to 15 Ma in the easternmost parts, indicating a Tertiary age of deformation (Wells et al., 2000). Apatite fission track ages record protracted, progressive west-to-east unroofing along the Raft River detachment fault between 13.6 and 7.4 Ma (Wells et al., 2000).

The RRSZ is almost entirely hosted in the Elba Quartzite and the overlying schist member, and the Raft River detachment fault follows the foliation in the schist member (Compton, 1972, 1975; Compton et al., 1977; Malavieille, 1987a; Wells, 2001). Strain associated with Tertiary extension dies out rapidly in the Archean rocks beneath the Elba Quartzite, and the boundary between the two has acted as a strain guide, concentrating Tertiary deformation in the quartzite (Sabisky, 1985; Malavieille, 1987a; Wells, 2001). Based on microstructural studies, Wells et al. (2000) and Wells (2001) recognized that deformation throughout the RRSZ is characterized by greenschist-facies conditions and that the base of the RRSZ is marked by an end of greenschist-facies retrograde metamorphism and deformation in the underlying Archean rocks. A series of north-vergent, transport-parallel recumbent folds some of which extend for 20 km or more along trend are present within the RRSZ in the southern Raft River Mountains (Fig. 1) (Compton, 1980; Sabisky, 1985; Malavieille, 1987a), but there is no evidence for folding of the Elba Quartzite in the northern Raft River Mountains.

Microstructural and quartz-*c*-axis-fabric studies have been conducted throughout the RRSZ by numerous workers (Compton, 1980; Sabisky, 1985; Malavieille, 1987a, 1987b; Wells, 1997, 2001). Kinematic indicators including type-II S-C fabrics, asymmetric tails on feldspar porphyroclasts, shear bands, mica fish, and asymmetric cross-girdle and single-girdle quartz *c*-axis fabrics (see reviews by Law, 1990; Hanmer and Passchier, 1991; Passchier and Trouw, 1996) all consistently indicate a component of top-to-the-east, normal-sense displacement along the RRSZ (Compton, 1980; Sabisky, 1985; Malavieille, 1987a, 1987b; Wells, 2001). Nearly symmetrical type-I cross-girdle quartz *c*-axis fabrics have also been reported from several areas in the RRSZ (Compton, 1980; Sabisky, 1985; this study), indicating that these areas record relatively large components of coaxial deformation (Lister and Hobbs, 1980; Schmid and Casey, 1986; Law, 1990). Wells (2001) independently showed that the RRSZ as a whole records a component of coaxial deformation that accommodates zone-normal contraction coupled with elongation in the transport direction.

The Elba Quartzite contains a variety of excellent strain markers including original quartz grains; quartz-pebble metaconglomerate; and local, basal quartz-cobble metaconglomerate. A number of workers have conducted three-dimensional strain analyses on these rocks (Fig. 2) (Compton, 1980; Sabisky, 1985; Malavieille, 1987a; Wells, 2001; this study). Results of these strain analyses show that strain intensity and strain geometry in the RRSZ vary considerably both along- and across-strike and with structural level (Compton, 1980; Sabisky, 1985; Malavieille, 1987a; Wells, 2001; this study). Strains in the constrictional field are almost entirely confined to the Clear Creek area in the northern half of the shear zone whereas flattening strains are predominately

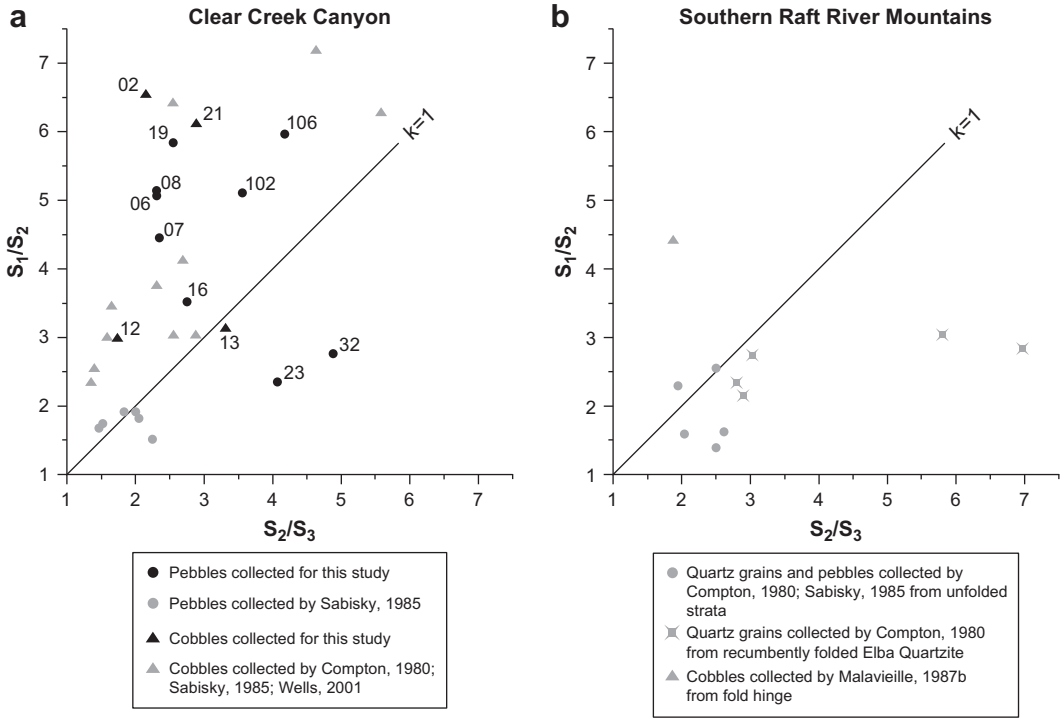

Fig. 2. (a) Flinn diagram showing all available strain data collected from the Clear Creek Canyon area (northern half) of the Raft River shear zone (RRSZ). (b) Flinn diagram showing all available strain data collected from the southern half of the RRSZ. Data originally compiled by Wells (2001).

confined to the southern half of the RRSZ and are often associated with the large-scale recumbent folds present in this area (Fig. 2) (Compton, 1980; Sabisky, 1985; Malavieille, 1987a; Wells, 2001; this study). In many areas strain intensity increases downwards, approaching the base of the Elba Quartzite (Compton, 1980; Sabisky, 1985; this study). Compton (1980) has also documented a transition from symmetric, cross-girdle quartz *c*-axis fabrics to asymmetric, single-girdle *c*-axis fabrics associated with this downward increase in strain intensity. Wells (2001) postulated that this transition represents an increasing component of noncoaxial deformation (see review by Law, 1990) due to the presence of a stretching fault (Means, 1989) at the base of the shear zone manifested by a domain of intense noncoaxial plastic deformation that accommodates transport-parallel elongation of the shear zone. Additionally, strain intensity at all structural levels increases from west to east, with measured ratios between the long and short axes of the finite-strain ellipsoid (R_{xz}) increasing from 2.6 at the western, up-dip end of the RRSZ to 35 or more in the eastern Raft River Mountains (Malavieille, 1987a; Wells, 2001). Wells (2001) documented an extreme case of this west-to-east increase in strain intensity along the north wall of Clear Creek canyon in the northeastern Raft River Mountains (Fig. 1) where R_{xz} values measured in the basal cobbles of the Elba Quartzite increase from 5.5 to 35 over a horizontal distance of only 700 m. Wells (2001) referred to this extreme finite-strain transition as the Clear Creek strain gradient, and this area is the focus of my detailed case study of finite-strain variations in the RRSZ.

3. Rock units

3.1. Footwall Archean rocks

Rocks of the Archean Green Creek complex, in the footwall of the RRSZ (Figs. 1, 3), record a complex pre-Tertiary deformational and metamorphic history. Understanding this history is an important part of interpreting the finite-strain variations observed in the overlying shear zone. One of the oldest units in the map area is a biotite schist that contains the mineral assemblage biotite + quartz + plagioclase + clinozoisite ± muscovite ± hornblende. The biotite schist exhibits a strong foliation and a variable mineral lineation defined by aligned biotite and quartz grains. This fabric is coeval with the dominant metamorphic assemblage. In places the biotite schist is extensively intruded by trondhjemite dikes, and it commonly contains numerous quartz veins. Both dikes and quartz veins show little internal deformation but are typically boudinaged parallel with the mineral lineation and, locally, perpendicular to the mineral lineation and parallel with the foliation. Scarce dikes and quartz veins that lie at a high angle to the foliation have been isoclinally folded with fold axial surfaces subparallel with the foliation. Approaching the RRSZ and the lower contact of the Elba Quartzite, the biotite schist is progressively overprinted by greenschist-facies retrograde metamorphism and coeval deformation, and the assemblage muscovite + chlorite + quartz + clinozoisite + Fe–Ti opaques ± tourmaline is developed in the RRSZ.

Interlayered and perhaps infolded with the biotite schist is a fine-grained hornblende schist that contains the assemblage hornblende + plagioclase + quartz + biotite + epidote + sphene that records epidote-amphibolite-facies metamorphic conditions. This unit locally exhibits relict fragmental texture indicating that it has a volcaniclastic protolith. Contacts between hornblende schist and biotite schist are locally gradational over ~20 cm. The hornblende schist typically contains a moderate to strong foliation and a well-defined hornblende mineral lineation that are coeval with epidote-amphibolite-facies metamorphism. Metatrondhjemite dikes and quartz veins hosted in these rocks show similar boudinage and folding relationships to those previously noted in the biotite schist.

The oldest intrusive unit in the map area consists of a series of coarse-grained metagabbro bodies that exhibit a relict igneous-intrusive texture. These rocks contain the assemblage hornblende + relict plagioclase + clinozoisite + metamorphic quartz + sphene + biotite that records epidote-amphibolite-facies metamorphic conditions, and they commonly contain a moderate to weak foliation at their margins. Metagabbro dikes intrude both the older schistose units, but were not observed intruding the metatrondhjemite described below.

The most prevalent intrusive unit in the map area is a metamorphosed and weakly deformed trondhjemite pegmatite containing the primary metamorphic assemblage plagioclase + quartz + muscovite. Compton (1975) reports that the muscovite is derived from potassium feldspar locally present in undeformed, unmetamorphosed trondhjemite bodies observed elsewhere in the Raft River Mountains. Metatrondhjemite dikes extensively intrude both of the older schistose units, but only intrude the metagabbro at one locality. Larger metatrondhjemite bodies are typically massive to weakly foliated and are commonly boudinaged parallel with the mineral lineation in the older schistose units. Dikes less than ~10-cm thick typically contain a strong foliation and lineation that are concordant with fabric elements in the surrounding metamorphic rocks.

Much of the Raft River Mountains are underlain by an extensive adamellite body that yielded a Rb–Sr whole-rock minimum age of 2180 ± 190 Ma (Compton, 1972, 1975; Compton et al., 1977). A potentially correlative adamellite orthogneiss in the Grouse Creek Mountains yielded a Rb–Sr whole-rock minimum age of 2510 ± 170 Ma, and upper intercepts on concordia for cores of zircons from the orthogneiss indicate an age of ~2620 Ma (Compton et al., 1977; Egger et al., 2003). Adamellite dikes intrude every unit described above, but do not intrude the overlying Elba Quartzite (Compton, 1972, 1975; Compton et al., 1977). In the area of this study, adamellite beneath the RRSZ typically contains a weak foliation. Quartz in these rocks exhibits sweeping grain-boundary-migration dynamic recrystallization (regime-III of Hirth and Tullis, 1992) whereas both plagioclase and potassium feldspar exhibit undulose extinction, and potassium feldspar has locally reacted to form muscovite. Where it is cut by the RRSZ, the adamellite is transformed into a mylonite. Quartz in mylonitic adamellite exhibits subgrain-rotation dynamic recrystallization (regime-II of Hirth

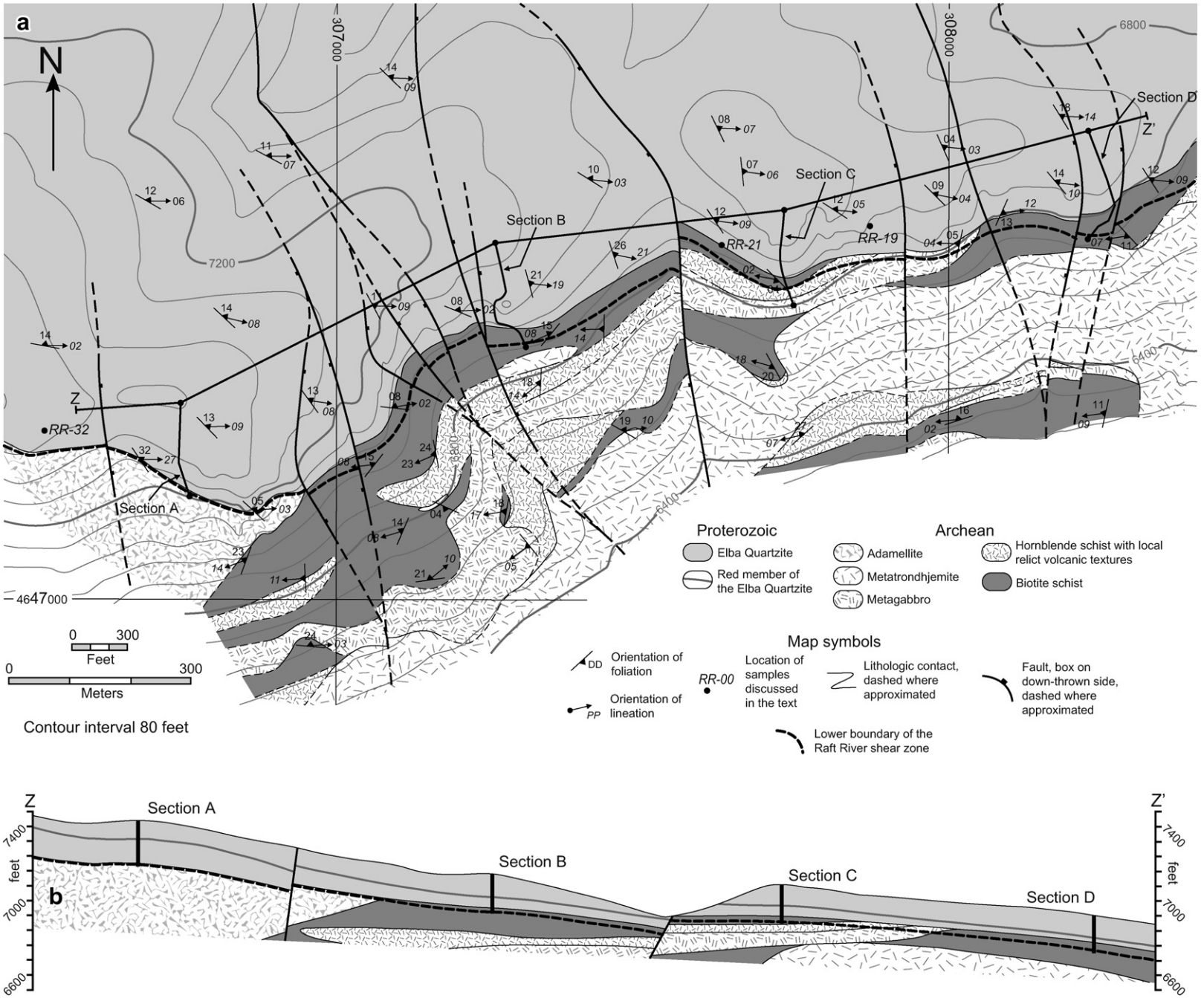

Fig. 3. (a) Geologic map of the Clear Creek strain gradient of the RRSZ. The locations of the lower boundary of the shear zone, the line of the cross section (Z–Z'), the measured sections displayed in Figs. 5 and 6, and the sample localities discussed in the text are noted. (b) Cross section along line Z–Z' in (a). The locations of measured sections presented in Figs. 5 and 6 are noted.

and Tullis, 1992) and feldspars are extensively converted to muscovite. At the base of the Elba Quartzite, the adamellite is converted into a phyllonite that is composed of >85% muscovite. It seems likely that at least part of this mylonite-to-phyllonite transition in adamellite cut by the RRSZ is a result of weathering of feldspars to clay minerals near the time of the deposition of the Elba Quartzite. However, the existence of well-rounded coarse-cobble metaconglomerate at the base of the Elba Quartzite indicates that at least the base of this unit was deposited in a very high-energy environment that would have completely removed any thick accumulations of clay soil, leaving the Elba Quartzite deposited on relatively unaltered igneous and metamorphic rocks. Therefore, I judge that the generation of phyllonites at this structural level was driven at least in part by chemical reactions and diffusive mass transfer that took place during Tertiary deformation.

3.2. Elba Quartzite

In the Clear Creek area, the Elba Quartzite contains a distinct stratigraphy that includes from bottom to top: (1) a local basal quartz-cobble metaconglomerate; (2) an interval of micaceous quartzite and subordinate muscovite-quartz schist; (3) a very distinct bed of red quartzite; (4) a distinct bed of coarse, white quartz-pebble metaconglomerate; (5) an interval of interbedded feldspar-quartz-pebble metaconglomerate, feldspathic quartzite, and muscovite-quartz schist; and (6) an upper interval of nearly pure, tan-to-white, cross-bedded quartzite. The overlying schist member of the Elba Quartzite is not preserved in the study area. The quartz-cobble metaconglomerate lies in a series of channels incised into the underlying Archean rocks. These channels can die out rapidly, with the cobble-metaconglomerate beds varying in thickness from 0 to 2 m or more over a lateral distance of 5–20 m. Both a complete lack of repetition of this distinct stratigraphy and the abundant cross-beds preserved in parts of the Elba Quartzite demonstrate that it has not been folded in the northern Raft River Mountains.

Throughout the study area, the Elba Quartzite contains a well-developed mesoscopic foliation defined by aligned muscovite and a quartz grain-shape fabric. A well-developed mineral lineation in these rocks is defined by streaking of muscovite domains on foliation surfaces, a quartz grain-shape fabric, and streaking on deformed quartz pebbles. The orientations of the long axes of stretched pebbles and cobbles do not deviate from the mineral lineation orientation in any systematic manner. Wells et al. (2000) and Wells (2001) noted that the Elba Quartzite is characterized by frictional/brittle deformation of feldspars and subgrain-rotation dynamic recrystallization of quartz (regime-II of Hirth and Tullis, 1992). They also note that deformed quartz grains exhibit subbasal deformation lamellae and that quartz *c*-axis fabrics exhibit maxima indicative of large components of basal slip in the $\langle a \rangle$ direction. My results confirm these observations, and all of these data point towards deformation under greenschist-facies conditions (White, 1976; Hirth and Tullis, 1992; Stipp et al., 2002).

3.3. Metamorphism and deformation predating the Raft River shear zone

The primary metamorphic and deformational event recorded in the Archean rocks in the immediate footwall of the RRSZ is manifested by the pervasive epidote-amphibolite-facies metamorphic assemblage and the deformation fabric defined by these metamorphic minerals. The absence of garnet in amphibolites constrains peak pressures during this event to ~6 kb or less (Spear, 1993). Deformation fabrics in the footwall of the RRSZ are characterized by northeast–southwest-striking, gently northwest-dipping foliations and west-southwest-trending mineral lineations (Fig. 4a). The observation that metatrondhjemite dikes and quartz veins hosted in biotite schist and hornblende schist throughout the study area are commonly boudinaged subparallel with and locally perpendicular to mineral lineations indicates that deformation in the footwall of the RRSZ is characterized by plane strain or strain in the flattening field wherein the maximum finite shortening direction is roughly defined by the poles to the foliations and the maximum finite elongation direction is roughly defined by the mineral lineations. It is also important to note that the adamellite pluton, the youngest unit in the footwall, contains only a weak foliation outside of the RRSZ indicating that there was little deformation after its emplacement. An upper age limit for metamorphism and deformation in the footwall of the RRSZ is given by $^{40}Ar/^{39}Ar$ spectra interpreted by Wells et al. (2000) as indicating maximum hornblende cooling ages of 54.6–90.5 Ma through the argon closure temperature (~500 °C).

4. Geometry of the Raft River shear zone in the study area

4.1. Data collection

To better understand the RRSZ in the area of the Clear Creek strain gradient, I mapped the shear zone and the underlying Archean rocks in detail (Fig. 3a) and measured a series of four detailed sections (A–D) through the shear zone along approximately strike-parallel routes (Figs. 3, 5, 6). In any locality with sufficient exposure, I made quantitative finite-strain estimates by measuring axial ratios of cobbles and pebbles in the Elba quartzite and then calculating harmonic means of these measurements. Measured faces were within 5° of the principal planes defined by the foliation and lineation. Lineation-perpendicular faces were measured at each locality and typically yielded 15–25 measurements. Depending on exposure, I also measured clasts on faces perpendicular to the foliation and parallel with the lineation and/or on foliation surfaces. Lineation-parallel faces typically yielded 10–15 measurements. Three lineation-perpendicular exposures of cobble metaconglomerate display a sufficient number of strain markers for collection of R_f/ϕ data (Lisle, 1985). These data were processed using the Microsoft Excel spreadsheet of Chew (2003) and do not show any statistically significant evidence for a pre-existing preferred orientation in the cobbles at these localities (Fig. 7). Unfortunately, throughout the study

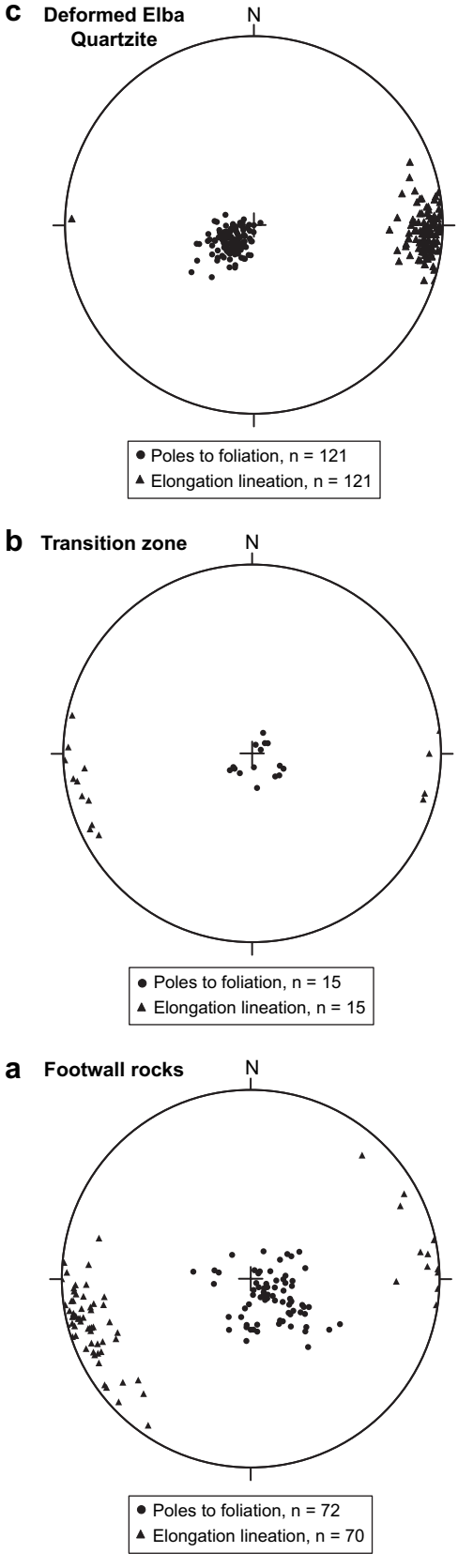

area, original quartz grains are too recrystallized to function as reliable strain markers.

I use two parameters to describe the measured finite-strain ellipsoids in the RRSZ. These are strain intensity and Flinn's (1962) strain geometry parameter. Strain intensity (i) is defined as

$$i = \sqrt{[(S_1/S_2) - 1]^2 + [(S_2/S_3) - 1]^2}$$

where S_1, S_2, and S_3 are the maximum, intermediate, and minimum principal stretches (van der Pluijm and Marshak, 2004). Flinn's parameter (k) is defined as

$$k = \frac{(S_1/S_2) - 1}{(S_2/S_3) - 1}$$

$k = 0$ for pure flattening strain, 1 for plane strain, and ∞ for pure constrictional strain (Flinn, 1962).

I collected oriented samples at intervals along the measured sections and at select other localities within the RRSZ and in the footwall of the shear zone. Oriented thin sections were made from cuts parallel with the lineation and perpendicular to the foliation. Thin sections from faces perpendicular to both the lineation and the foliation and faces parallel with the foliation were also cut from several samples. There is no evidence of multiple deformation fabrics or lineation-parallel micro-folds in these sections.

4.2. Geometry of the lower boundary of the Raft River shear zone

Following Wells (2001), I mapped the lower boundary of the RRSZ as the lower limit of greenschist-facies retrograde metamorphism and associated deformation (Fig. 3). In the westernmost part of the study area, where the Elba Quartzite is underlain by adamellite, this boundary is only 2–5 m below the base of the quartzite (Fig. 3). Where the Elba Quartzite overlies more easily altered and deformed schistose rocks, in the central and eastern parts of the study area, the lower boundary of the shear zone extends 10–15 m below the nonconformity (Fig. 3). At the easternmost end of the study area, shear zone fabrics extend 20–25 m below the base of the Elba Quartzite (Fig. 3). Foliations in this transition zone between the highly deformed Elba Quartzite and the unaltered Archean rocks are subhorizontal to northeast–southwest-striking and gently northwest-dipping, and mineral lineations trend east-west to west-southwest (Fig. 4b). This foliation orientation is slightly oblique to the overall northwest–southeast-striking, gently northeast-dipping shear zone boundary, and this sense of obliquity is similar to that expected for the margins of a gently northeast-dipping,

Fig. 4. (a) Orientations of foliations and lineations from the Archean igneous intrusive rocks and amphibolite-facies metamorphic rocks in the footwall of the RRSZ. (b) Orientations of foliations and lineations from the zone of Tertiary greenschist-facies retrograde metamorphism and deformation in the Archean rocks just beneath the Elba Quartzite at the lower boundary of the RRSZ. (c) Orientations of foliations and lineations from the Elba Quartzite in the main body of the RRSZ. All plots are equal-area, lower-hemisphere projections.

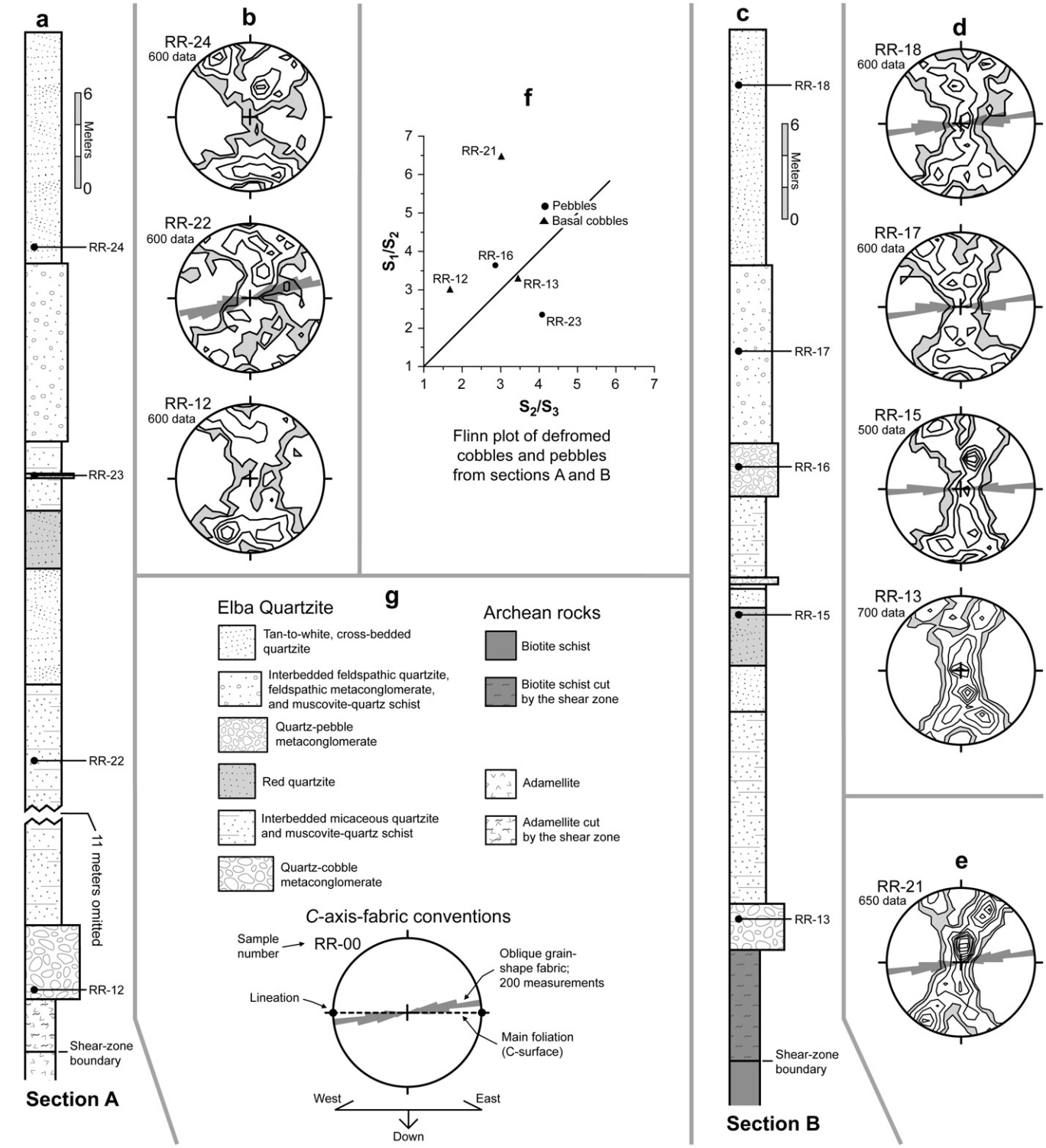

Fig. 5. Measured sections/sampling transects through the RRSZ and quartz *c*-axis fabrics from the western half of the study area. Locations of sections are given in Fig. 3. (a) Section A showing lithologic units and sample locations. (b) Quartz *c*-axis fabrics from section A. (c) Section B showing lithologic units and sample locations. (d) Quartz *c*-axis fabrics from section B. (e) Quartz *c*-axis fabric from sample RR-21 collected from the quartz-cobble metaconglomerate between sections B and C (Fig. 3). (f) Quantitative strain estimates from sections A and B. (g) Key to lithologic units in the measured sections and display conventions for the quartz *c*-axis fabrics in (b), (d), and (e). C-axis fabrics are displayed perpendicular to the foliation and parallel with the lineation in equal-area, lower-hemisphere projections, and they are viewed towards north. Contours are 0.5, 1, 2, …, 7-times uniform density. For samples with an oblique grain-shape fabric defined by recrystallized quartz grains (type-II S-C fabric), 200 measurements of the angle between the long axis of recrystallized quartz grains and the main foliation (c-surface) are given as directional data in the center of the quartz *c*-axis-fabric plots.

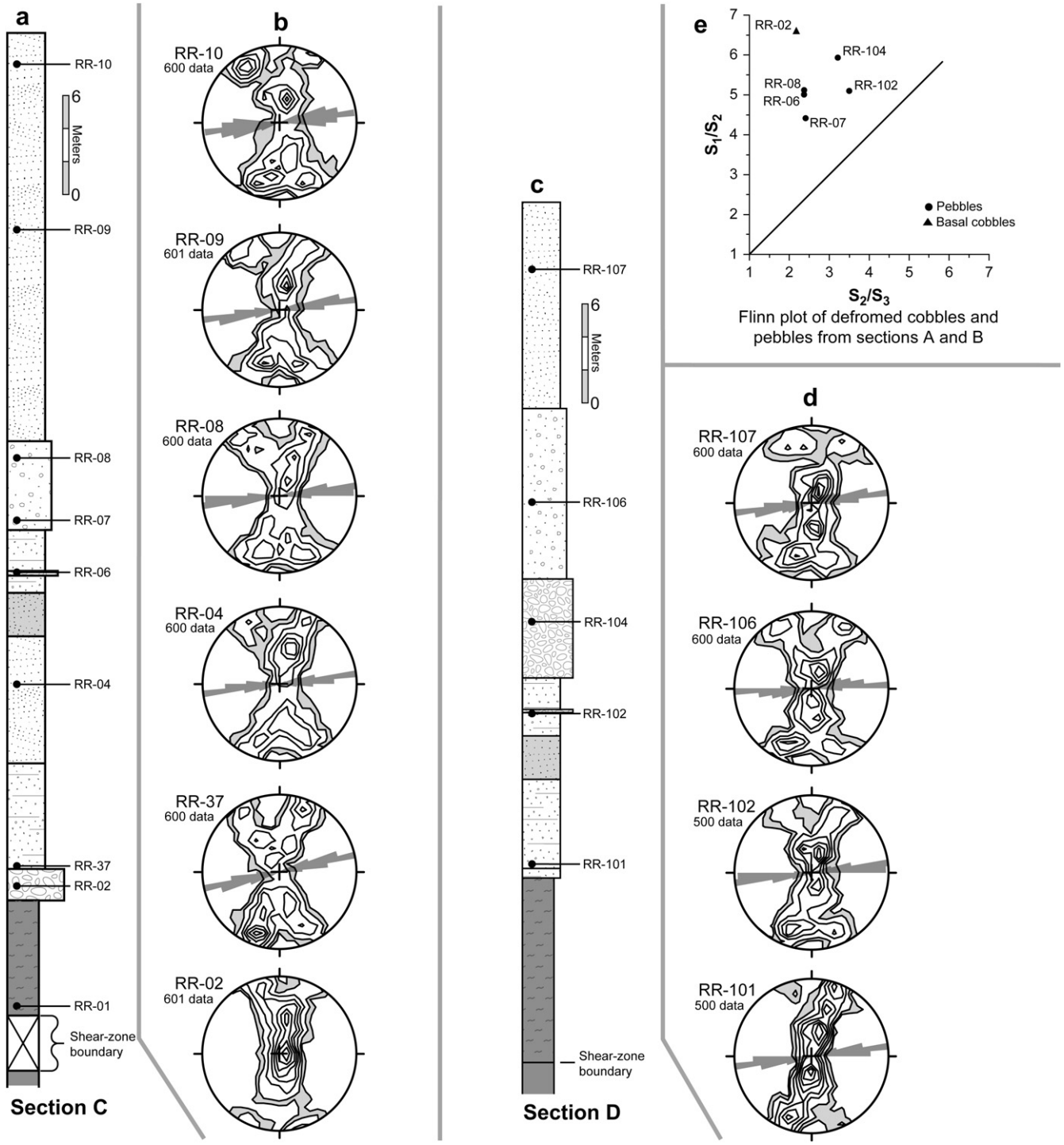

Fig. 6. Measured sections/sampling transects through the RRSZ and quartz *c*-axis fabrics from the eastern half of the study area. Locations of sections are given in Fig. 3. (a) Section C showing lithologic units and sample locations. (b) Quartz *c*-axis fabrics from section C. (c) Section D showing lithologic units and sample locations. (d) Quartz *c*-axis fabrics from section D. (e) Quantitative strain estimates from sections C and D. The key to the lithologic units in the measured sections and the display conventions for the quartz *c*-axis fabrics in (b) and (d) are given in Fig. 5g. *C*-axis fabrics are displayed perpendicular to the foliation and parallel with the lineation in equal-area, lower-hemisphere projections, and they are viewed towards north. Contours are 0.5, 1, 2, …, 7-times uniform density. For samples with an oblique grain-shape fabric defined by recrystallized quartz grains (type-II S-C fabric), 200 measurements of the angle between the long axis of recrystallized quartz grains and the main foliation (c-surface) are given as directional data in the center of the quartz *c*-axis-fabric plots.

top-to-the-east shear zone (sensu Ramsay and Graham, 1970). High-strain rocks in the transition zone derived from biotite schist and hornblende schist are also characterized by well-developed, centimeter-scale shear bands (Fig. 8a). Mylonites derived from adamellite typically exhibit both S-C fabrics (Berthé et al., 1979) and well-developed shear bands (Berthé et al., 1979; Platt and Vissers, 1980) that often overprint S-C fabrics. In all cases, these structures indicate top-to-the-east displacement.

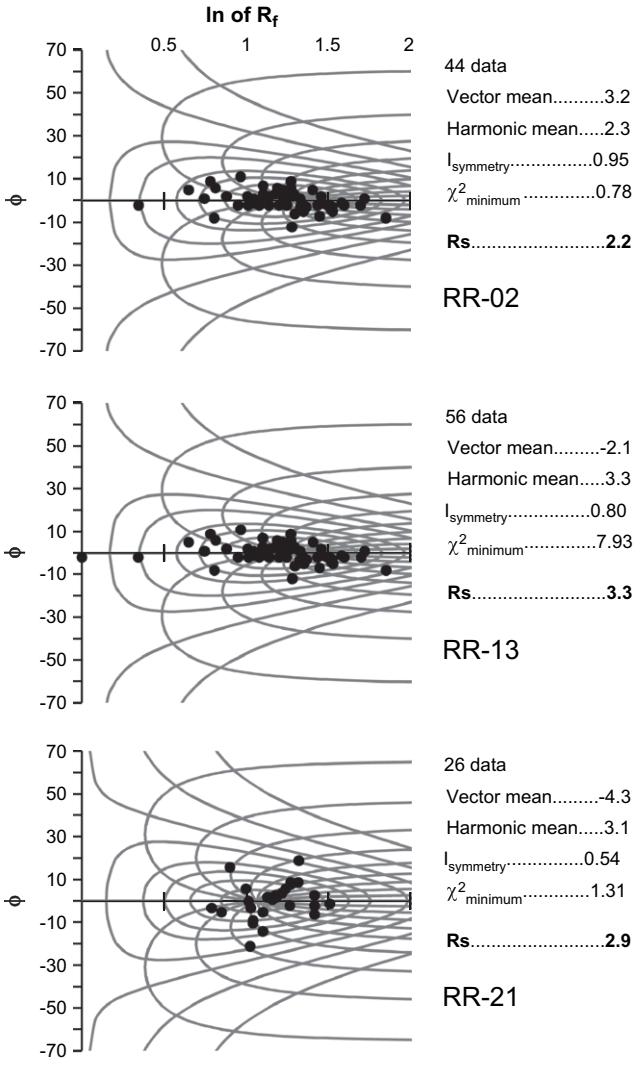

Fig. 7. R_f/ϕ data collected from the basal cobble metaconglomerates on faces normal to the lineation and the foliation. RR-13 lies at the base of the Elba Quartzite in section B (Figs. 3, 5c). RR-21 lies at the base of the Elba Quartzite between sections B and C (Fig. 3). RR-02 lies at the base of the Elba Quartzite in section C (Figs. 3, 6a).

4.3. Fabric geometry and finite-strain variations in the Elba Quartzite

Foliations in the Elba Quartzite strike northwest–southeast and dip gently to the northeast, and mineral lineations are east-trending and gently plunging (Fig. 4c). Bedding is parallel with the foliation. The measurements presented in Fig. 4c would be even more consistent had minor misorientations not been introduced by the north-northwest–south-southeast-striking, steeply dipping, frictional/brittle high-angle normal faults that cut the RRSZ fabrics throughout the study area (Fig. 3a). Shear bands (Berthé et al., 1979; Platt and Vissers, 1980) indicating top-to-the-east displacement are commonly developed in the thin muscovite-quartz-schist beds that are present in parts of the Elba Quartzite (Fig. 8b), and most samples of the Elba Quartzite exhibit weak type-II S-C fabrics (Lister and Snoke, 1984), also indicating top-to-the-east displacement.

All of the finite-strain data collected for this study are presented in Fig. 2a, Fig. 9, and Table 1. As noted by Wells (2001) strain intensity increases significantly from west-to-east, and this increase is accompanied by a corresponding thickness decrease in the Elba Quartzite (Figs. 3b, 5, 6, 9). Throughout most of the study area, finite strains lie in the constrictional field (Figs. 2a, 9). However, flattening strains were measured at two localities in the area of section A at the extreme western end of the study area in the thin, coarse-quartz-pebble-metaconglomerate bed of the Elba Quartzite (Figs. 2a, 3a, 9). Additionally, qualitative observations of strain geometry made using exposures of quartz-pebble metaconglomerates that do not allow quantitative measurements indicate that this domain of strain in the flattening field extends throughout the far western end of the study area. Localities that lie furthest into the constrictional field are located in the area of section C (Fig. 9) where k values from pebble metaconglomerates in the center of the Elba Quartzite range from 2.5 to 3.0 and the cobble metaconglomerate at the base of the Elba Quartzite yields a k value of 4.6; the most prolate strain geometry recorded in the study area. This downwards increase in constrictional strain at section C is accompanied by an overall increase in strain intensity from $i = 3.8–4.4$ in the pebble metaconglomerates in the center of the Elba Quartzite to $i = 5.7$ in the cobble metaconglomerate at the base of the quartzite. Two other cobble metaconglomerate localities, RR-12 ($k = 2.8$) at the base of section A and RR-21 ($k = 2.7$) between sections B and C, and one other pebble metaconglomerate locality, RR-19 ($k = 3.1$) east of section C, also deviate well into the constrictional field (Figs. 2a, 3a, 9). Elsewhere, quantitative estimates of Flinn's parameter were ≤ 1.8. To summarize, strain intensity increases abruptly between sections B and C, and this increase is directly associated with a transition from strain in the flattening field in the far western end of the field area to plane strain at section B to strain in the constrictional field in the intensely deformed eastern half of the study area. Within the resolution of my data, there is no correlation between strain intensity and the degree of deviation from plane strain (Fig. 2a; Table 1). There does, however, appear to be a correlation between structural level and strain geometry. With one exception (RR-13 at the base of section B), finite-strain estimates from the basal cobble metaconglomerate lie well into the constrictional field, even in the area of section A where strain estimates from higher structural levels indicate flattening strains (Figs. 5, 6, 9).

5. Quartz *c*-axis fabric analyses

I measured quartz c-axis fabrics in samples taken from throughout the study area using a universal stage (Figs. 5, 6). The fabrics become progressively stronger from the relatively low-strain western end of the study area to the intensely deformed eastern end. Throughout the area they typically form weakly asymmetric cross girdles that are indicative of: (1) a general-shear deformation history involving significant components of coaxial strain (Lister and Hobbs, 1980; Schmid and Casey, 1986; Law, 1990) and (2) a strain geometry that does

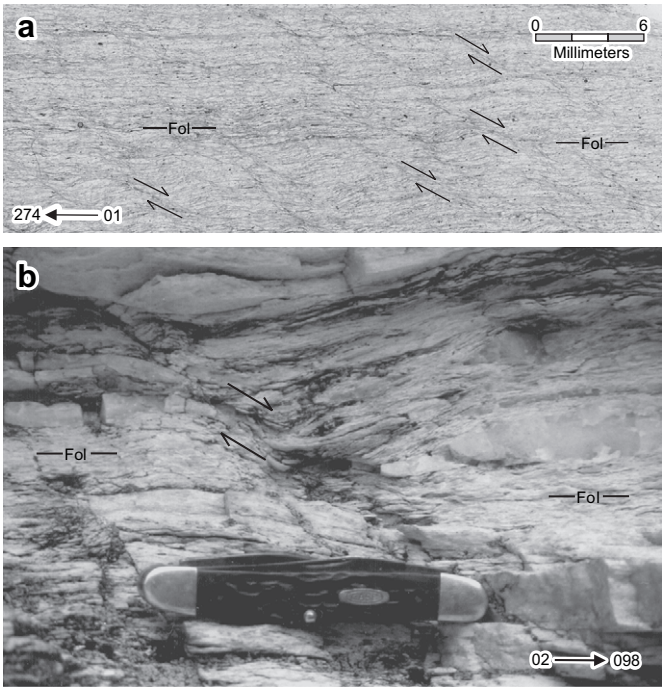

Fig. 8. (a) Scanned thin section displaying shear bands that indicate a top-to-the-east sense-of-shear. The sample (RR-01) was collected in section C (Figs. 3, 6a). (b) Photograph of a shear band in a thin bed of muscovite-quartz schist in the Elba Quartzite between sections C and D that indicates a top-to-the-east sense-of-shear. Pocketknife for scale is 9.8-cm long. Both images are viewed towards north, perpendicular to the subhorizontal foliation and parallel with the mineral lineation. Lineation orientation is indicated on the images.

not deviate very far from plane strain (Tullis et al., 1973; Tullis, 1977; Lister et al., 1978; Lister and Hobbs, 1980; Price, 1985; Law, 1986). Strongly asymmetric cross-girdle fabrics and/or single-girdle fabrics were recorded near the base and top of section D (samples RR-101 and RR-107, Fig. 6d) and in the basal cobble metaconglomerate between sections B and C (sample RR-21, Figs. 3a, 5e). Within the study area, only two samples yielded quartz *c*-axis patterns that may be interpreted as transitional between plane strain and either constrictional strain or flattening strain. The first of these is sample RR-02 ($k = 4.6$) collected from the cobble metaconglomerate at the base of section C (Fig. 6b). This sample shows a widening of the central girdle and a corresponding tightening of the arms of the cross girdle relative to the immediately overlying samples that can be interpreted as transitional between a plane-strain, type-I-cross-girdle fabric and the double-girdle fabric (with girdles symmetrical about the lineation) that is expected for coaxial, constrictional deformation (Lister and Hobbs, 1980; Price, 1985). Conversely, sample RR-24 which lies in the area of flattening strain at the top of section A (Fig. 5b) shows a weakening of the central segment of the cross girdle and a strengthening of the small-circle girdles that are indicative of flattening strain (Lister and Hobbs, 1980; Price, 1985; Law, 1986).

Because the central girdles of the quartz *c*-axis fabrics collected from this area are roughly centered about the intermediate finite-strain axis and lie at a high angle to both the foliation and the lineation, these samples record an approximately monoclinic deformation symmetry. This argument is based on the observation that quartz crystallographic fabrics will form in response to the external kinematic framework imposed upon the sample and therefore record the flow plane and direction of the coaxial component of deformation and the shear plane and direction of the noncoaxial component of deformation (Wallis, 1992, 1995; Sullivan and Law, 2007). This argument is supported by: (1) numerical simulations of quartz crystallographic-fabric formation (Lister and Hobbs, 1980; Wenk et al., 1989; Jessell and Lister, 1990), (2) quartz and analogue-material deformation experiments (Tullis, 1977; Bouchez and Duval, 1982; Herwegh and Handy, 1996; Takeshita et al., 1999), and (3) observations of naturally deformed samples (Law et al., 1990). Note, however, that recent experimental work by Heilbronner and Tullis (2006) indicates that this relationship may not hold true for samples undergoing grain-boundary-migration dynamic recrystallization (regime-III of Hirth and Tullis, 1992).

6. Kinematic vorticity analyses

6.1. Overview of strain-path variations and kinematic vorticity analysis

A useful measure of the degree of noncoaxiality of flow is the kinematic vorticity number (W_k) (Truesdell, 1954; see also reviews by Means et al., 1980; Tikoff and Fossen, 1995). For the simple case of two-dimensional deformation with no net external rotation, a simplified version of W_k can be defined as the cosine of the angle between the flow apophyses (Means et al., 1980). For monoclinic deformations showing no external rotation, W_k will range from zero (cosine 90°) for coaxial deformation to one (cosine 0°) for the case of strict simple shear. The intermediate case, or roughly equal contributions of pure shear and simple shear, occurs at $W_k = 0.71$ (cosine 45°). In the past two decades a number of workers have developed useful methods for quantitatively estimating W_k in naturally deformed rocks (e.g. Passchier, 1987, 1988; Wallis, 1992, 1995; Fossen and Tikoff, 1993; Simpson and De Paor, 1993; Jessup et al., 2007). I have conducted kinematic vorticity analyses on suitable samples to provide a more detailed picture of how coaxial and noncoaxial components of deformation are distributed throughout the area of this study and related to variations in strain intensity and strain geometry. These analyses include: (1) the quartz-*c*-axis-fabric/oblique-grain-shape method of Wallis (1995), (2) the quartz-*c*-axis-fabric/finite-strain method of Wallis (1992, 1995), and (3) the rigid-grain-rotation method of Passchier (1987, 1988) modified by Wallis et al. (1993). Each of these methods utilizes data collected on two-dimensional section planes, and the analyses, as they are applied here, are not strictly valid for the non-plane-strain deformations recorded in the RRSZ. However, Tikoff and Fossen (1995, p. 1776–1777) have shown that two-dimensional kinematic-vorticity analyses of three-dimensional, monoclinic deformations will consistently overestimate W_k by only a small amount. The overestimation will be greatest for nearly equal

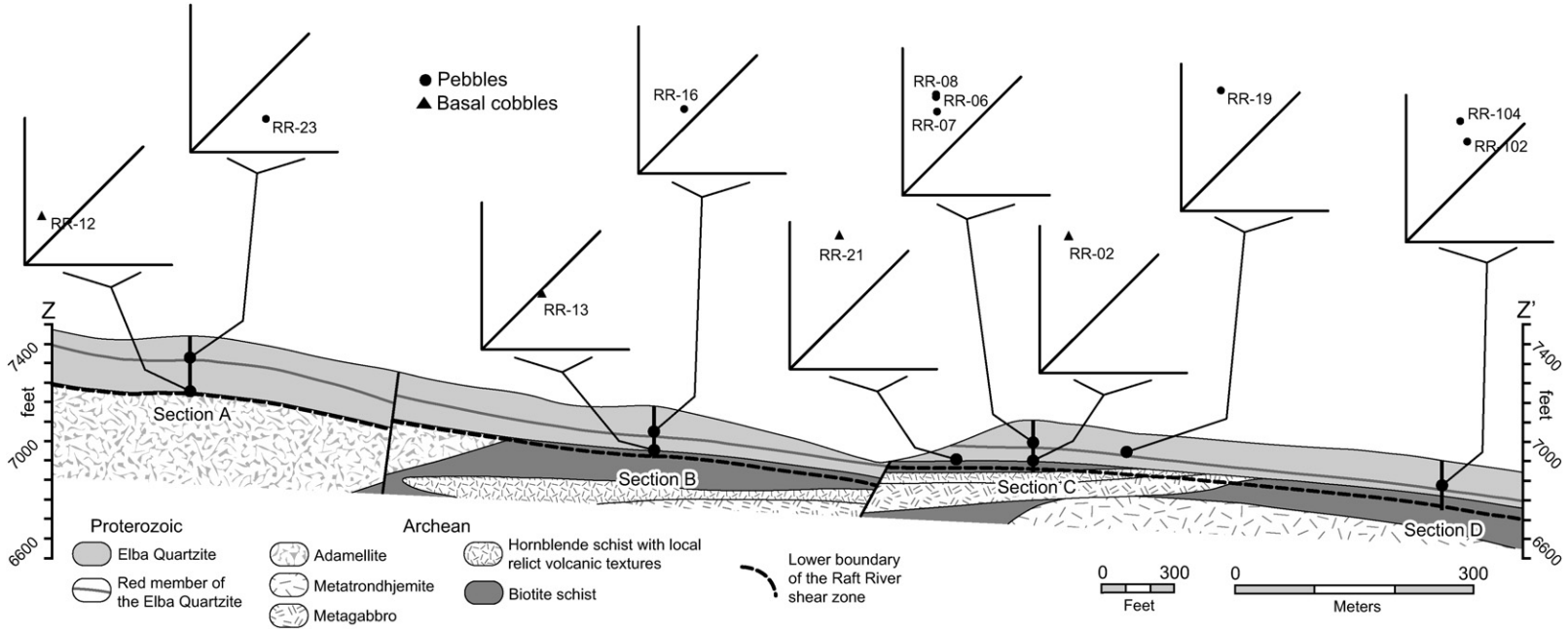

Fig. 9. Spatial comparison of finite-strain data along cross section $Z{-}Z'$ (Fig. 3) using simplified Flinn diagrams. Note the west-to-east increase in strain intensity and the concentration of strain in the constrictional field in the area of section C.

Table 1
Table reporting finite-strain estimates collected for this study

Sample	S_1/S_2	S_2/S_3	i	k
RR-32	2.8	4.9	4.3	0.4
Section A				
RR-23	2.4	4.1	3.4	0.4
RR-12	3.0	1.7	2.1	2.8
Section B				
RR-16	3.5	2.8	3.1	1.4
RR-13	3.2	3.3	3.1	0.9
RR-21	6.2	2.9	5.5	2.7
Section C				
RR-08	5.1	2.4	4.4	2.9
RR-07	4.4	2.4	3.7	2.5
RR-06	5.0	2.4	4.2	3.0
RR-02	6.6	2.2	5.7	4.6
RR-19	5.9	2.6	5.1	3.1
Section D				
RR-104	5.9	3.7	5.6	1.8
RR-102	5.1	3.5	4.8	1.6

The data are arranged from west to east by measured section and from top to bottom within each section (Figs. 3a, 5, 6).

components of coaxial and noncoaxial deformation and will decline to zero as W_k goes to zero or one. For the strain intensities encountered in the RRSZ, this overestimation will be ≤ 0.06. The methodology, inherent assumptions, and results of each of these methods are considered in turn below.

6.2. Method 1, quartz c-axis fabrics and oblique grain shape

For any monoclinic deformation, there is a direct relationship between the instantaneous stretching direction and W_k (Means et al., 1980; Tikoff and Fossen, 1995). Realizing this, Wallis (1992, 1995) has argued that the central girdle of a quartz *c*-axis fabric will form at a near-right angle to the flow plane of the coaxial component of deformation and the shear plane of the noncoaxial component of deformation and can therefore be used to define the kinematic framework of the deformed sample. Wallis (1995) has also argued that neoblasts within a steady-state, dynamically recrystallizing aggregate (e.g. oblique grain-shape fabric of a type-II S-C fabric) will nucleate with their long axes at or near the maximum instantaneous stretching direction and then rotate towards parallelism with the flow plane/shear plane as deformation proceeds. Based on these assumptions, W_k can be estimated using the relationship

$$W_k = \sin[2(\beta + \alpha)]$$

where β is the angle between the main foliation and the pole to the leading edge of the central segment of the quartz *c*-axis fabric and α is the largest angle between the long axis of any recrystallized grain in the oblique grain-shape fabric and the main foliation (Wallis, 1995). Because this measurement of W_k utilizes incremental-strain features, it records only the last stages of deformation. As a result, one must assume steady-state deformation in order to use this method for estimating the mean vorticity of deformation (W_m) experienced by the sample throughout its deformation history. Conversely, this method can be used to examine the last episode of deformation in polydeformed rocks provided that the quartz crystallographic fabric has been completely reset from any earlier deformation history. The results of these analyses and the values of β and α used are given in Table 2.

6.3. Method 2, quartz c-axis fabrics and finite strain

For any monoclinic deformation, the long axis of the finite-strain ellipsoid will rotate towards parallelism with the flow plane of the coaxial component and the shear plane of the noncoaxial component of deformation. The axis of this rotation is the vorticity vector (Wallis, 1992, 1995; Fossen and Tikoff, 1993). Thus, any combination of finite-strain intensity and the angle between the long axis of the finite-strain ellipsoid and the flow plane/shear plane uniquely defines a value of W_m (Fossen and Tikoff, 1993; Tikoff and Fossen, 1995). Using Wallis' (1992, 1995) assumption that the central girdle of a quartz *c*-axis fabric will form perpendicular to the flow plane/shear plane, it is possible to calculate a value of W_k using the angle β and the strain ratio measured in the *XZ* plane (R_{xz}), or the plane perpendicular to the foliation and parallel with the lineation, using the following equation (Wallis, 1992, 1995).

$$W_k = \sin\left\{\arctan\left[\frac{\sin(2\beta)}{\left(\frac{R_{xz}+1}{R_{xz}-1}\right) - \cos(2\beta)}\right]\right\} \times \left(\frac{R_{xz}+1}{R_{xz}-1}\right)$$

This measurement of W_k utilizes the total finite strain experienced by the sample, and it is therefore susceptible to error induced by the existence of a pre-existing preferred orientation (e.g. sedimentary fabric or earlier deformation history) in the strain markers used to estimate R_{xz}. Also, because quartz *c*-axis fabrics used to estimate the orientation of the flow plane/shear plane require a significant amount of finite strain to develop or to be reset (Lister and Williams, 1979; Hobbs, 1985; Law, 1990), they likely record a large component of the deformation history experienced by the sample. However, it cannot be demonstrated that they record the entire deformation history, especially for large strain intensities. Hence, though this kinematic vorticity analysis method represents a larger sampling of the strain history of a given sample, it may not record the entire deformation history and therefore may not be an accurate estimate of W_m if deformation is non-steady state. This method is also inherently inaccurate for large finite-strain intensities because, for R_{xz} values greater than about 10, small variations in the angle β will yield large changes in the estimated value of W_k (Graseman et al., 1999). This is the source of the large uncertainties associated with the method 2 analyses. The results of these analyses and the values of β and R_{xz} used in the calculations are given in Table 2.

Table 2
Values of kinematic vorticity calculated for this study and the parameters used to calculate them

Sample	β_{Min}	β_{Max}	α_{Max}	R_{xz}	W_k oblique grain shape (1)	W_k strain ratio (2)	W_k rigid object (3)
Section A							
RR-12	2	4		4.0		0.17–0.33	
Section B							
RR-18	1	2	24		0.77–0.79		
RR-17	6	12	21		0.81–0.91		0.70–0.73
RR-15	6	10	21		0.81–0.88		
RR-13	0	2		10.1		0–0.37	
RR-21	8	12	26	16.2	0.93–0.97	0.96–1.00	
Section C							
RR-10	2	6	27		0.85–0.91		
RR-09	3	6	23		0.79–0.85		0.77–0.80
RR-08	2	5	19	10.7	0.67–0.74	0.38–0.75	
RR-04	4	5	24		0.83–0.85		
RR-37	0	2	31		0.88–0.91		
RR-02	0	2		12.3		0–0.43	
Section D							
RR-107	8	12	34		0.99–1.00		
RR-106	3	7	27		0.87–0.93		0.76–0.83
RR-102	2	4	24	17.0	0.79–0.83	0.54–0.81	
RR-101	6	10	29		0.94–0.98		

The data are arranged from west to east by measured section and from top to bottom within each section (Figs. 5, 6).

6.4. Method 3, rigid-grain rotation

The rotation of rigid objects of varying aspect ratios in a viscously deforming matrix is a function of both the viscosity contrast between the objects and the matrix and the degree of noncoaxiality (Passchier, 1987; Simpson and De Paor, 1993). By assuming that the viscosity contrast is significantly large enough to be a negligible factor and that there are no local viscosity asperities between the rotating objects and the matrix (e.g. mica caps on porphyroclasts), it is possible to estimate W_k by determining the axial ratio at which clasts are no longer able to rotate, or the critical axial ratio (R_c), using the equation below (Passchier, 1987, 1988; Wallis et al., 1993).

$$W_k = \frac{(R_c^2 + 1)}{(R_c^2 - 1)}$$

Like the quartz-*c*-axis-fabric/oblique-grain-shape method, this method for estimating W_k is limited to analyzing the last increments of deformation, and can therefore be used to analyze the last deformation event in polydeformed samples, as any change in the incremental deformation history will result in a reorientation of the rotating rigid objects and a new R_c value. The results of these analyses as well as the axial-ratio data are given in Fig. 10 and Table 2.

6.5. Results of kinematic vorticity analyses

The results of each of the three methods used to estimate W_k are compared in Fig. 11. By examining these data, several important trends become evident. To begin, the average value of W_k for all of the samples is 0.74, and the average value of all of the samples excluding the basal cobble metaconglomerate is 0.81. As discussed above, these values overestimate W_k by as much as 0.06 (Tikoff and Fossen, 1995). Therefore, these data indicate that the Elba Quartzite in the study area records approximately 50–60% noncoaxial deformation. Second, method 1 typically gives higher estimates of W_k than methods 2 and 3 in those samples for which multiple analysis methods can be used, but all three methods generally agree to within 15% or less (Fig. 11; Table 2). Third, three-out-of-four samples collected from the basal cobble metaconglomerate (RR-02, RR-12, and RR-13) yield significantly lower W_k values than samples collected from the overlying quartzite mylonites, and these are the only samples that experienced a pure-shear-dominated deformation history. Fourth, there is a transition between section B where values of W_k above the basal metaconglomerate remain relatively constant with structural level and sections C and D where the base and the top of the Elba Quartzite are characterized by larger components of noncoaxial deformation (Fig. 11). This transition corresponds with the distinct increase in strain intensity between section B and sections C and D and it is most pronounced in section D where the largest average strain intensity is recorded (Figs. 9, 11). It also corresponds with the shift from slightly asymmetric cross-girdle quartz *c*-axis fabrics to the single-girdle and asymmetric cross-girdle fabrics at the base and top of section D.

7. Potential models

7.1. Overprinting deformation events and/or sedimentary fabrics

One possible explanation for the observed variations in strain intensity and strain geometry in the RRSZ is that the final state of strain is a result of multiple overprinting

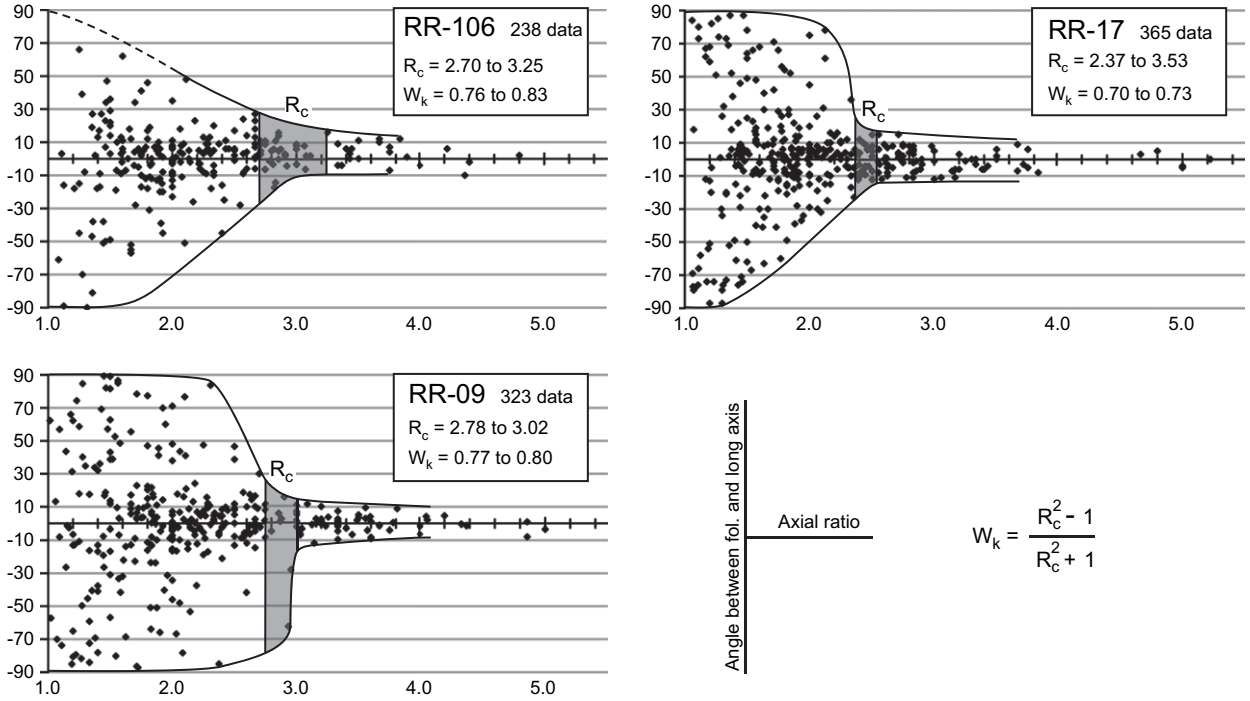

Fig. 10. Data used in the rigid-grain-rotation kinematic-vorticity-analysis method (method 3). Rigid grains are feldspar porphyroclasts in the quartzite mylonites. The estimated range of R_c for each sample is indicated by the gray field. Sample RR-106 is from section D, sample RR-09 is from section C, and sample R-17 is from section B (Figs. 3a, 5c, 6a,c).

deformation events and/or the existence of an initial depositional shape-preferred orientation (e.g. imbricated clasts) within the finite-strain markers used in this study. This hypothesis is supported by the existence of an extensive pre-Tertiary record of penetrative, plastic deformation and metamorphism in the Albion-Raft River-Grouse Creek metamorphic core complex, including rocks fabrics in the immediate footwall of the RRSZ described above. However, it ultimately seems unlikely for a variety of reasons. First, the pre-Tertiary deformation history recorded in the underlying Archean rocks is characterized by plane strain or strain in the flattening field with axes of the bulk finite-strain ellipsoid that are subparallel with the fabric elements in Fig. 4a. That is, the long axis of the finite-strain ellipsoid is west-southwest-trending and gently plunging, the intermediate axis is north-northwest-trending and gently plunging and the short axis is south-southeast-trending and steeply plunging. If Tertiary deformation were strongly constrictional, the overprinting hypothesis would be an excellent fit with my data. However, the quartz *c*-axis fabrics demonstrate that Tertiary deformation must be near plane strain throughout most of the RRSZ. Overprinting of a plane-strain or flattening-strain ellipsoid oriented parallel with the footwall fabric elements (Fig. 4a) with a plane-strain ellipsoid oriented with its principal axes parallel with the fabric elements in the Elba Quartzite (Fig. 4c) will not produce a bulk finite-strain ellipsoid in the constrictional field like those recorded throughout much of the study area. Second, the R_f/ϕ analyses conducted on the basal cobble metaconglomerate on sections perpendicular to both the foliation and lineation (*YZ* sections) yield I_{symmetry} and χ^2 values from symmetry tests that are insufficient to reject the null hypothesis of no initial preferred orientation in the deformed elliptical markers for the available sample sizes (Lisle, 1985). In other words, these tests do not show any statistically valid evidence for an initial preferred orientation within the basal Elba cobbles. This observation helps rule out the possibility of a depositional preferred orientation in these strain markers. However, the tests for sample RR-21 are close to showing compelling evidence for an initial preferred orientation, and this sample has an unsatisfactorily small sample size (Borradaile, 1984). Therefore, I consider it to be questionable. Finally, the quartz-*c*-axis-fabric/strain-ratio kinematic-vorticity-analysis method will overestimate W_k if any previous deformation history increases the axial ratio of strain markers used in the analysis. That is, if an earlier deformation event not recorded by the quartz *c*-axis fabrics increases R_{xz} used in these analyses, they will give anomalously high W_k estimates. Because this method generally gives lower estimates of W_k than the other methods employed (Fig. 11) and the principal strain axes of the earlier deformation fabric beneath the shear zone are close to parallel with the axes of the Tertiary deformation ellipsoid, these data also argue against any strong pre-existing preferred orientation of strain markers in the RRSZ. The exception to this is, once again, sample RR-21 where the quartz-*c*-axis-fabric/strain-ratio kinematic-vorticity analysis yields a larger estimate of W_k than the quartz-*c*-axis-fabric/oblique-grain-shape-fabric method. Based on these observations it seems likely that the basal Elba cobbles at locality RR-21 did indeed have a strong pre-existing preferred orientation, but this is the only location in the study area for which this argument can be made.

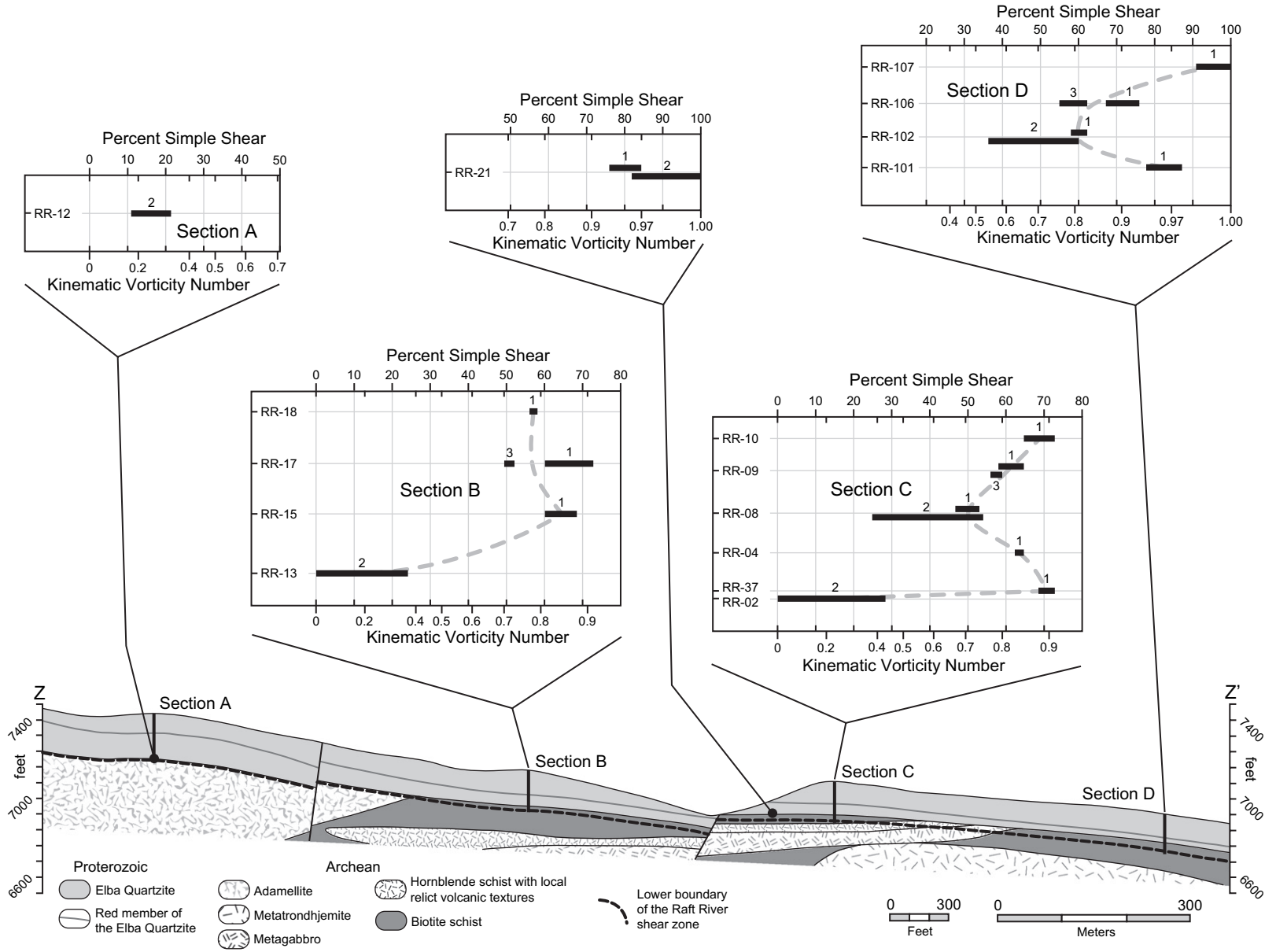

Fig. 11. Charts comparing estimated values of kinematic vorticity from each of the three methods discussed in the text. Method 1 is the quartz-*c*-axis-fabric/oblique-grain-shape method, method 2 is the quartz-*c*-axis-fabric/finite-strain method, and method 3 is the rigid-grain-rotation method. The data are arranged from west to east along cross section *Z*–*Z*′ (Fig. 3), and the vertical spacing in the plots is roughly scaled to the actual vertical sample spacing.

Volume change during deformation can also affect the shape of the finite-strain ellipsoid (Ramsay and Wood, 1973). In the Elba Quartzite, the dominance of crystal-plastic deformation indicated by the subgrain-rotation-recrystallization microstructure (Hirth and Tullis, 1992) and a general paucity of microstructural evidence for solution transfer both indicate approximate constant-volume deformation. However, significant volume loss probably occurred in the mylonitized and phyllonitized adamellite and the retrograde metamorphosed schist units at the base of the shear zone.

Since there is no compelling evidence for a significant pre-Tertiary shape-preferred orientation in the RRSZ in the area of the Clear Creek strain gradient, it seems that the observed variations in both strain intensity and strain geometry are a primary feature of Tertiary extensional deformation associated with core complex exhumation. This apparent lack of significant pre-Tertiary deformation in the Elba Quartzite indicates that much of the penetrative deformation recorded in the footwall rocks must be Archean in age. Such an observation agrees with the earlier observation that the youngest footwall unit, the adamellite, contains only a weak foliation outside of the RRSZ.

7.2. Three-dimensional deformation partitioning and necking of the Raft River shear zone

The data presented above show that the RRSZ in this area is characterized by nearly equal components of coaxial and noncoaxial strain accommodating simultaneous top-to-the-east displacement and shortening across the shear zone coupled with elongation in the transport direction. As noted by Wells (2001), the Clear Creek strain gradient represents an extreme case of a general west-to-east increase in strain intensity in the RRSZ. This increase is directly associated with: (1) a change in rock type in the immediate footwall of the RRSZ from adamellite to biotite schist (Fig. 3); (2) a change in strain geometry from strain in the flattening field to plane strain to strain in the constrictional field as strain intensity increases from west-to-east (Figs. 2a, 3a, 9); and (3) a change in the flow geometry, with the component of coaxial deformation being localized in the center of the Elba Quartzite in the more intensely deformed areas of the RRSZ (Fig. 11). All of these observations are incorporated into the conceptual kinematic model presented in Fig. 12. In this model, the Clear Creek strain gradient represents a zone of necking within the RRSZ due to a severe increase in both top-to-the-east displacement accommodated by plastic deformation and transport-parallel elongation of the shear zone. Because the intensity of Tertiary deformation dies out rapidly downwards, a stretching fault must exist between the Elba Quartzite in the main body of the RRSZ and the Archean metamorphic and igneous rocks in the footwall (Wells, 2001). The microstructural and kinematic-vorticity data indicate that this stretching fault must be localized in the Archean rocks at the base of the RRSZ that have undergone greenschist-facies retrograde metamorphism and penetrative deformation as well as in the base of the Elba Quartzite in the eastern-most parts of the study area. The extensively developed top-to-the-east shear bands in the highly deformed schistose rocks cut by the stretching fault just beneath the Elba Quartzite record a component of transport-parallel elongation which dies out structurally downwards as deformation decreases. This allowed strain compatibility to be maintained throughout the shear zone without requiring a single large displacement across any one surface. In this proposed geometry, the rheology of the Archean metamorphic and intrusive igneous rocks that are cut by the stretching fault at the base of the RRSZ directly controlled the amount of coaxial strain that could accumulate in the overlying shear zone by limiting the amount of transport-parallel elongation that could occur. In the area of the Clear Creek strain gradient, the intensely deformed rocks in the east are underlain by biotite schist that is readily deformed under greenschist-facies conditions whereas the weakly deformed rocks in the west are underlain by adamellite that is comparatively rheologically strong under greenschist-facies conditions until a thoroughgoing network of rheologically weak minerals is formed (Tullis, 2002; Holyoke and Tullis, 2006). Therefore, because of this rheological transition and the associated ease of concentrating noncoaxial strain at the base of the Elba Quartzite, the eastern parts of the study area were able to accommodate the component of zone-normal contraction coupled with elongation in the transport direction both earlier in the deformation history and to a greater extent than areas to the west that are underlain by adamellite. These assertions agree with predictions made by many theoretical studies, numerical simulations, and observations of naturally deformed rocks indicating that noncoaxial deformation will be partitioned into rheologically weak domains such as schist layers within lithologically heterogeneous deformation zones (e.g., Lister and Williams, 1983; Jiang, 1994a, b; Goodwin and Williams, 1996; Goodwin and Tikoff, 2002). A similar top-to-the-east plastic stretching fault is also inferred to exist at the top of the Elba Quartzite where it would primarily be localized in the overlying schist member that is no longer exposed in the study area. Displacement on this stretching fault and/or the overlying frictional/brittle detachment fault must increase to the west in order to accommodate the larger component of top-to-the-east displacement recorded in the eastern part of the Elba Quartzite.

The transition in strain geometry from strain in the flattening field and plane strain in the western half of the study area to strain in the constrictional field in the eastern half of the study area is directly correlated with the transport-parallel increase in strain intensity. Therefore, I also interpret this strain-geometry transition as being driven by the rheological transition in the rocks that are cut by the stretching fault that controls the increase in strain intensity (Fig. 12). In this interpretation, the constrictional strains in the eastern half of the study area represent strike-parallel flow of material into the area of extreme transport-parallel elongation over the relatively weak biotite schist. Lateral flow into highly extended domains in an extensional tectonic setting may in part be driven by local decreases in the lithostatic load over the highly extended domains driving lateral flow from adjacent

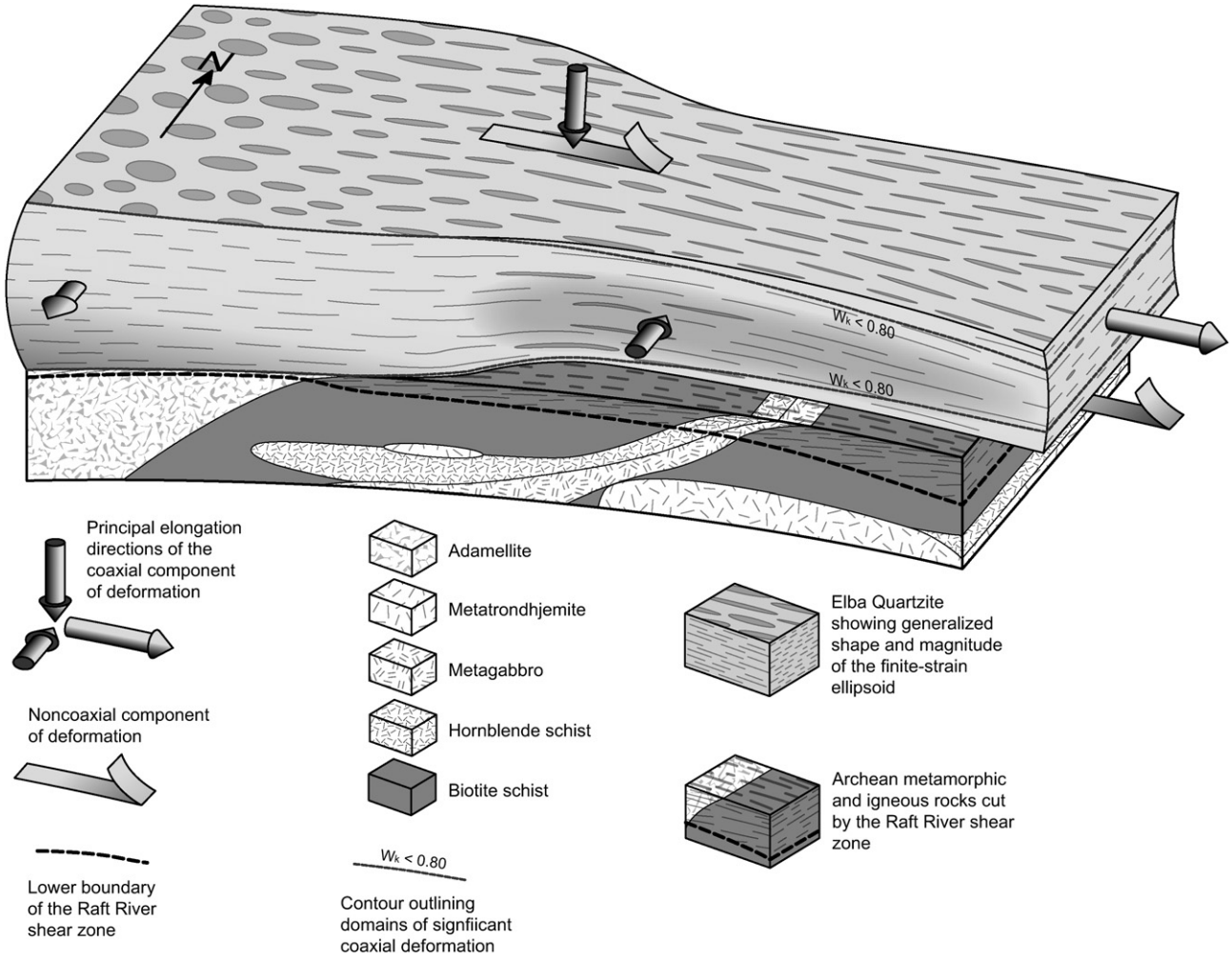

Fig. 12. Block-diagram cartoon showing the geometry of the RRSZ in the area of the Clear Creek strain gradient as developed from the map data, strain data, and kinematic-vorticity data discussed in the text. The pattern in the Elba Quartzite is generalized and intended to represent both the relative strain intensity and strain geometry.

less-extended domains with a greater lithostatic load (Fletcher and Bartley, 1994; Fletcher et al., 1995). The flattening strains recorded in the western end of the field area where the RRSZ is directly underlain by adamellite may record lateral flow into adjacent highly extended domains. Alternatively, they may have developed in order to accommodate shear-zone-normal shortening while minimizing the component of noncoaxial strain needed in the stretching fault at the base of the shear zone to accommodate this shortening in any one direction. These mechanisms are not mutually exclusive. Either interpretation requires the stretching fault at the base of the RRSZ to exhibit a triclinic symmetry in areas of the shear zone that have not experienced plane-strain deformation because components of strike-perpendicular and strike-parallel noncoaxial deformation are needed to accommodate both elongation of the shear zone parallel with the transport direction and the strike-parallel shortening or elongation. Outside of the basal stretching fault, a nearly monoclinic deformation symmetry may still be maintained in the main body of the RRSZ. This model does not require the RRSZ to record bulk strain in the constrictional field because local constrictional strains may be balanced by flattening strains in adjacent parts of the shear zone. Regional evidence for such a balance is given by the occurrence of predominately flattening strains in the southern half of the shear zone (Fig. 2b).

Rheologically driven strain-path partitioning can also explain the localized development of highly prolate strain geometries in the quartz-cobble metaconglomerates at the base of the Elba Quartzite. As outlined above, the cobble metaconglomerates occur in distinct channel-form bodies (likely original sedimentary channels) incised into the underlying Archean metamorphic and igneous rocks. Throughout the study area, the enveloping Archean rocks have undergone extensive retrograde metamorphism, and are converted to phyllonites immediately below the Elba Quartzite. The cobble-metaconglomerate beds are inferred to be rheologically stronger than the enveloping phyllonites. Kinematic vorticity analyses of the cobble metaconglomerates indicate that they record a pure-shear-dominated deformation history (Fig. 11, Table 2). The phyllonites, on the other hand, display abundant microstructural evidence for a strongly noncoaxial deformation history. Therefore, the shear zone at this structural level records rheologically driven

strain-path partitioning wherein the cobble metaconglomerates preferentially absorb the component of transport-parallel elongation and any component of strike-parallel shortening (bulk constrictional strain), and the enveloping phyllonites accommodate the component of noncoaxial deformation. This model does not work well for the basal cobble metaconglomerate at locality 21 which records constrictional strain and a highly noncoaxial deformation history. However, locality 21 is also the only spot that exhibits compelling evidence for a pre-existing shape-preferred orientation in the basal Elba cobbles. This can explain the development of a prolate finite-strain ellipsoid under near-simple-shear, plane-strain conditions.

8. Summary and conclusions

Detailed geologic mapping, strain analyses, quartz-*c*-axis-fabric analyses, and kinematic-vorticity analyses in the Clear Creek area of the RRSZ enable the reconstruction of an extreme west-to-east, along-transport gradient in finite-strain intensity associated with a shift in the shape of the finite-strain ellipsoid from the flattening field into the constrictional field. These data show that the Clear Creek strain gradient represents necking of the shear zone that is associated with both an increase in top-to-the-east displacement and zone-normal shortening coupled with elongation in the transport direction. A stretching fault that accommodates transport-parallel elongation of the shear zone is largely localized in a domain of greenschist-facies retrograde metamorphism and intense deformation at the nonconformity that separates the Elba Quartzite in the main body of the shear zone from the underlying Archean igneous and metamorphic rocks. In this geometry, the rheology of the Archean rocks cut by the stretching fault directly controls the amount and style of zone-normal shortening and transport-parallel elongation that can take place. The domain of intense deformation and necking of the shear zone is localized above rheologically weak biotite schist that is easily deformed under greenschist-facies conditions and can therefore accommodate large amounts of transport-parallel elongation of the shear zone. This domain is also characterized by strain in the constrictional field caused by strike-parallel flow into the domain of extreme transport-parallel elongation from surrounding parts of the shear zone. Rheologically driven strain-path partitioning also led to the development of strongly constrictional strains in cobble metaconglomerate at the base of the Elba Quartzite. These metaconglomerates preferentially absorb the coaxial, constrictional component of deformation whereas the rheologically weaker phyllonites that surround them accommodate the noncoaxial component of deformation. At the western end of the field area, where the footwall Archean rocks are rheologically stronger, the RRSZ records significantly lower strain intensities. Flattening strains in this area may have developed because the zone-normal shortening was partitioned into components of both strike-parallel and strike-perpendicular elongation in order to limit the amount of stretching needed in any one direction and/or because material was moving into adjacent highly extended domains. This model does not require bulk strain in the constrictional field, as there is regional evidence that local domains of constrictional strain may be balanced by adjacent domains of flattening strain. These observations demonstrate how localized rheological transitions can control the partitioning of deformation in a crustal-scale structure and ultimately help control the way the crust behaves during large-scale extensional deformation.

Acknowledgements

This work was supported by a grant from the Geological Society of America and by the University of Wyoming Department of Geology and Geophysics. This detailed study would not have been possible without the excellent range-scale characterization of the RRSZ provided by R.R. Compton, M.L. Wells, and others. A.W. Snoke is thanked for introducing me to the area. I completed this work while in residence at the University of Wyoming, and B.R. Frost, S.T. Jackson, B.E. John, R.D. Law, and A.W. Snoke provided helpful informal reviews while serving on my PhD examining committee. The manuscript was further improved by formal reviews from J.M. Fletcher and S. Giorgis, but any remaining errors of omission or interpretation are my own.

References

Armstrong, R.L., 1968. Mantled gneiss domes in the Albion Mountains, southern Idaho. Geological Society of America Bulletin 79, 1295–1314.

Bailey, C.M., Francis, B.E., Fahrney, E.E., 2004. Strain and vorticity analysis of transpressional high-strain zones from the Virginia Piedmont, USA. In: Alsop, G.I., Holdsworth, R.E., McCaffrey, K.J.W., Hand, M. (Eds.), Flow Processes in Faults and Shear Zones, vol. 224. Geological Society, London, pp. 249–264. Special Publications.

Berthé, D., Choukroune, P., Gapais, D., 1979. Orthogneiss mylonite and noncoaxial deformation of granites: the example of the South Armorican shear zone. Journal of Structural Geology 1, 31–42.

Borradaile, G.J., 1984. Strain analysis of passive elliptical markers: success of de-straining methods. Journal of Structural Geology 6, 433–437.

Bouchez, J.L., Duval, P., 1982. The fabric of polycrystalline ice deformed in simple shear: experiments in torsion, natural deformation and geometrical interpretation. Textures and Microstructures 5, 171–190.

Chew, D.M., 2003. An Excel spreadsheet for finite strain analysis using the *R*f/ϕ technique. Computers and Geosciences 29, 795–799.

Compton, R.R., 1955. Trondhjemite batholith near Bidwell Bar, California. Geological Society of America Bulletin 66, 9–44.

Compton, R.R., 1972. Geologic map of the Yost quadrangle, Box Elder County, Utah and Cassia County, Idaho. US Geologic Survey Miscellaneous Investigation Map I-672, scale 1:31,680.

Compton, R.R., 1975. Geologic map of the Park Valley quadrangle, Box Elder County, Utah and Cassia County, Idaho. US Geologic Survey Miscellaneous Investigation Map I-873, scale 1:31,680.

Compton, R.R., 1980. Fabrics and strains in quartzites of a metamorphic core complex, Raft River Mountains, Utah. In: Crittenden, Coney, P.J., Davis, G.H. (Eds.), Cordilleran Metamorphic Core Complexes. Geological Society of America Memoir, vol. 153, pp. 271–279.

Compton, R.R., Todd, V.R., Zartman, R.E., Naeser, C.W., 1977. Oligocene and Miocene metamorphism, folding, and low angle faulting in northwest Utah. Geological Society of America Bulletin 88, 1237–1250.

Coney, P.J., 1980. Cordilleran metamorphic core complexes: an overview. In: Crittenden Jr., M.D., Coney, P.J., Davis, G.H. (Eds.), Cordilleran Metamorphic Core Complexes. Geological Society of America Memoir, vol. 153, pp. 7–31.

Czeck, D.M., Hudleston, P.J., 2003. Testing models for obliquely plunging lineations in transpression: a natural example and theoretical discussion. Journal of Structural Geology 25, 959–982.

Dewey, J.F., 2002. Transtension in arcs and orogens. International Geology Review 44, 402–439.

Egger, A.E., Dumitru, T.A., Miller, E.L., Savage, C.F.I., 2003. Timing and nature of Tertiary plutonism and extension in the Grouse Creek Mountains, Utah. International Geology Review 45, 497–532.

Fletcher, J.M., Bartley, J.M., 1994. Constrictional strain in a non-coaxial shear zone: implications for fold and rock fabric development, central Mojave metamorphic core complex, California. Journal of Structural Geology 16, 555–570.

Fletcher, J.M., Bartley, J.M., Martin, M.W., Glazner, A.F., Walker, D.J., 1995. Large-magnitude continental extension: an example from the central Mojave metamorphic core complex. Geological Society of America Bulletin 107, 1468–1483.

Flinn, D., 1962. On folding during three-dimensional progressive deformation. Geological Society of London Quarterly Journal 118, 385–433.

Flinn, D., 1992. Comment on ''Ophiolitic mylonites in the Lizard complex: ductile extension in the lower oceanic crust''. Geology 19, 954.

Fossen, H., Tikoff, B., 1993. The deformation matrix for simultaneous simple shearing, pure shearing and volume change, and its application to transpression-transtension tectonics. Journal of Structural Geology 14, 413–422.

Giorgis, S., Tikoff, B., 2004. Constraints on kinematics and strain from feldspar porphyroclast populations. In: Alsop, I., Holdsworth, R. (Eds.), Transport and Flow Processes in Shear Zones, vol. 224. Geological Society, London, pp. 265–285. Special Publication.

Goodwin, L.B., Tikoff, B., 2002. Competency contrast, kinematics, and the development of foliations and lineations in the crust. Journal of Structural Geology 24, 1065–1085.

Goodwin, L.B., Williams, P.F., 1996. Deformation path partitioning within a transpressive shear zone, Marble Cove, Newfoundland. Journal of Structural Geology 18, 975–990.

Graseman, B., Fritz, H., Vannay, J.C., 1999. Quantitative kinematic flow analysis from the Main Central Thrust Zone (NW-Himalaya, India); implications for a decelerating strain path and the extrusion of orogenic wedges. Journal of Structural Geology 25, 19–34.

Hacker, B.R., Mosenfelder, J.L., 1996. Metamorphism and deformation along the emplacement thrust of the Samail ophiolite. Oman. Earth and Planetary Science Letters 144, 435–451.

Hanmer, S., Passchier, C.W., 1991. Shear-sense indicators: a review. Geological Survey of Canada, Paper, 90–117.

Heilbronner, R., Tullis, J., 2006. Evolution of c-axis pole figures and grain size during dynamic recrystallization: results from experimentally sheared quartzite. Journal of Geophysical Research 111, B10202, doi:10.1029/2005JB004194.

Herwegh, M., Handy, M.R., 1996. The evolution of high temperature mylonitic microfabrics: evidence for simple shearing of a quartz analogue (norcamphor). Journal of Structural Geology 18, 689–710.

Hirth, G., Tullis, J., 1992. Dislocation creep regimes in quartz aggregates. Journal of Structural Geology 14, 145–160.

Hobbs, B.E., 1985. The geological significance of microfabric analysis. In: Wenk, H.R. (Ed.), Preferred Orientations in Deformation Metals and Rocks: an Introduction to Modern Textural Analysis. Academic Press, Orlando, FL, pp. 463–479.

Holdsworth, R.E., Strachran, R.A., Dewey, J.F. (Eds.), 1998, Continental Transpressional and Transtensional Tectonics, vol. 135. Geological Society, London. Special Publication.

Holst, T.B., Fossen, H., 1987. Strain distribution in a fold in the West Norwegian Caledonides. Journal of Structural Geology 9, 915–924.

Holyoke, C.W., Tullis, J., 2006. Mechanisms of weak phase interconnection and the effects of phase strength contrast on fabric development. Journal of Structural Geology 28, 621–640.

Hossack, J.R., 1968. Pebble deformation and thrusting in the Bygdin area (southern Norway). Tectonophysics 5, 315–339.

Hudleston, P.J., 1999. Strain compatibility in shear zones: is there a problem? Journal of Structural Geology 21, 932.

Jessell, M., Lister, G.S., 1990. A simulation of the temperature dependence of quartz fabrics. In: Knipe, R.J., Rutter, E.H. (Eds.), Deformation Mechanisms, Rheology and Tectonics, vol. 54. Geological Society, London, pp. 353–362. Special Publication.

Jessup, M.J., Law, R.D., Frassi, C., 2007. The rigid grain net (RGN): an alternative method for estimating mean kinematic vorticity number (W_m). Journal of Structural Geology 29, 411–421.

Jiang, D., 1994a. Vorticity determination, distribution, partitioning and the heterogeneity and non-steadiness of natural deformations. Journal of Structural Geology 16, 121–130.

Jiang, D., 1994b. Flow variation in layered rocks subjected to bulk flow of various kinematic vorticities: theory and geological implications. Journal of Structural Geology 16, 1159–1172.

Jones, R.R., Holdsworth, R.E., Clegg, P., McCaffrey, K., Tavarnelli, E., 2004. Inclined transpression. Journal of Structural Geology 26, 1531–1548.

Law, R.D., 1986. Relationships between strain and quartz crystallographic fabrics in the Roche Maurice quartzites of Plougastel, western Brittany. Journal of Structural Geology 8, 493–515.

Law, R.D., 1990. Deformation Mechanisms, Rheology and Tectonics. In: Knipe, R.J., Rutter, E.H. (Eds.), Crystallographic fabrics: a selective review of their applications to research in structural geology, vol. 54. Geological Society, London, pp. 335–352. Special Publication.

Law, R.D., Schmid, S.M., Wheeler, J., 1990. Simple shear deformation and quartz crystallographic fabrics: a possible natural example from the Torridon area of NW Scotland. Journal of Structural Geology 12, 29–45.

Lin, S., Jiang, D., 2001. Using along-strike variation in strain and kinematics to define the movement direction of curved transpressional shear zones: an example from northwestern Superior Province, Manitoba. Geology 29, 767–770.

Lisle, R.J., 1985. Geological Strain Analysis: A Manual for the Rf/ϕ Technique. Pergamon Press, Oxford, 99 pp.

Lister, G.S., Hobbs, B.E., 1980. The simulation of fabric development during plastic deformation and its application to quartzite: the influence of deformation history. Journal of Structural Geology 2, 355–370.

Lister, G.S., Snoke, A.W., 1984. S-C mylonites. Journal of Structural Geology 6, 617–638.

Lister, G.S., Williams, P.F., 1979. Fabric development in shear zones, theoretical controls and observed phenomena. Journal of Structural Geology 1, 283–297.

Lister, G.S., Williams, P.F., 1983. The partitioning of deformation in flowing rock masses. Tectonophysics 92, 1–33.

Lister, G.S., Patterson, M.S., Hobbs, B.E., 1978. The simulation of fabric development during plastic deformation and its application to quartzite: the model. Tectonophysics 45, 107–158.

Malavieille, J., 1987a. Extensional shearing deformation and kilometer-scale ''a''-type folds in a cordilleran metamorphic core complex (Raft River Mountains, northwest Utah). Tectonics 6, 423–448.

Malavieille, J., 1987b. Kinematics of compressional and extensional ductile shearing deformation in a metamorphic core complex of the northeastern Basin and Range. Journal of Structural Geology 9, 541–554.

Means, W.D., 1989. Stretching faults. Geology 17, 893–896.

Means, W.D., Hobbs, B.E., Lister, G.S., Williams, P.F., 1980. Vorticity and non-coaxiality in progressive deformations. Journal of Structural Geology 2, 371–378.

Miller, D.M., 1980. Structural geology of the northern Albion Mountains, south-central Idaho. In: Crittenden, M.D., Coney, P.J., Davis, G.H. (Eds.), Cordilleran Metamorphic Core Complexes. Geological Society of America Memoir, vol. 153, pp. 399–423.

Moores, E.M., Twiss, R.J., 1995. Tectonics. W.H. Freeman and Company, New York, 415 pp.

Passchier, C.W., 1987. Stable positions of rigid objects in non-coaxial flow – a study in vorticity analysis. Journal of Structural Geology 9, 679–690.

Passchier, C.W., 1988. Analysis of deformation paths in shear zones. Geologisches Rundschau 77, 309–318.

Passchier, C.W., Trouw, R.A.J., 1996. Microtectonics. Springer-Verlag, New York, 289 pp.

Pfiffner, O.A., Ramsay, J.G., 1982. Constraints on geological strain rates: arguments from finite strain states of naturally deformed rocks. Journal of Geophysical Research 87, 311–321.

Platt, J.P., Vissers, R.L.M., 1980. Extensional structures in anisotropic rocks. Journal of Structural Geology 2, 397–410.

Price, J.P., 1985. Preferred orientations in quartzites. In: Wenk, H.R. (Ed.), Preferred Orientations in Deformation Metals and Rocks: An Introduction to Modern Texture Analysis. Academic Press, Orlando, FL, pp. 385–406.

Ramsay, J.G., Graham, R.H., 1970. Strain variation in shear belts. Canadian Journal of Earth Sciences 7, 786–813.

Ramsay, J.G., Wood, D.S., 1973. The geometric effects of volume change during deformation processes. Tectonophysics 16, 263–277.

Sabisky, M.A., 1985. Finite strain, ductile flow, and folding in the central Raft River Mountains, northwest Utah. MS thesis, University of Utah.

Schmid, S.M., Casey, M., 1986. Complete fabric analysis of some commonly observed quartz c-axis patterns. American Geophysical Union Geophysical Monograph 36, 263–286.

Simpson, C., De Paor, D.G., 1993. Strain and kinematic analysis in general shear zones. Journal of Structural Geology 15, 1–20.

Snoke, A.W., Miller, D.M., 1988. Metamorphic and tectonic history of the northeastern great basin. In: Ernst, W.G. (Ed.), Metamorphism and Crustal Evolution of the Western United States. Prentice-Hall, Englewood Cliffs, NJ, pp. 606–648.

Solar, G.S., Valentino, D.W., 2003. L-tectonites; what do they tell us about deformation history? Geological Society of America Abstracts with Program 35, no. 6, 181.

Spear, F.S., 1993. Metamorphic phase equilibria and pressure-temperature-time paths. Mineralogical Society of America, Washington, DC, 799 pp.

Stipp, M., Stünitz, H., Heilbronner, R., Schmid, S.M., 2002. Dynamic recrystallization of quartz: correlation between natural and experimental conditions. In: de Meer, S., Drury, M.R., de Bresser, J.H.P., Pennock, G.M. (Eds.), Deformation Mechanisms, Rheology and Tectonics: Current Status and Future Perspectives, vol. 200. Geological Society, London, pp. 171–190. Special Publication.

Strine, M., Wojtal, S.F., 2004. Evidence for non-plane strain flattening along the Moine Thrust, Loch Srath nan Aisinnin, north-west Scotland. Journal of Structural Geology 26, 1755–1772.

Sullivan, W.A., 2006. Structural significance of L tectonites in the eastern-central Laramie Mountains, Wyoming. Journal of Geology 114, 513–531.

Sullivan, W.A., Law, R.D., 2007. Deformation path partitioning within the transpressional White Mountain shear zone, California and Nevada. Journal of Structural Geology 29, 583–598.

Sullivan, W.A., Snoke, A.W., 2007. Comparative anatomy of core-complex development in the northeastern Great Basin. USA Rocky Mountain Geology 42, 1–29.

Takeshita, T., Wenk, H.R., Lebensohn, R., 1999. Development of preferred orientation and microstructure in sheared quartzite: comparison of natural data and simulated results. Tectonophysics 312, 133–155.

Tikoff, B., Fossen, H., 1995. The limitations of three-dimensional kinematic vorticity analysis. Journal of Structural Geology 17, 1771–1784.

Tikoff, B., Greene, D.C., 1997. Stretching lineations in transpressional shear zones: an example from the Sierra Nevada batholith, California. Journal of Structural Geology 19, 29–39.

Todd, V.R., 1980. Structure and petrology of a Tertiary gneiss complex in northwestern Utah. In: Crittenden, M.D., Coney, P.J., Davis, G.H. (Eds.), Cordilleran Metamorphic Core Complexes. Geological Society of America Memoir, vol. 153, pp. 349–383.

Truesdell, C., 1954. The Kinematics of Vorticity. Indiana University Press, Bloomington, IN, 232 pp.

Tullis, J., 1977. Preferred orientation of quartz produced by slip during plane strain. Tectonophysics 39, 87–102.

Tullis, J., 2002. Deformation of granitic rocks: experimental studies and natural examples. In: Karato, S., Wenk, H. (Eds.), Plastic Deformation of Minerals and Rocks. Reviews in Mineralogy and Geochemistry, 51, pp. 51–95.

Tullis, J., Christie, J.M., Griggs, D.T., 1973. Microstructures and preferred orientations in experimentally deformed quartzites. Geological Society of American Bulletin 84, 297–314.

Twiss, R.J., Moores, E.M., 1992. Structural Geology. W.H. Freeman and Company, New York, 532 pp.

van der Pluijm, B.A., Marshak, S., 2004. Earth Structure: An Introduction to Structural Geology and Tectonics. W.W. Norton and Company, New York, 656 pp.

Wallis, S.R., 1992. Vorticity analysis in a metachert from the Sanbagawa Belt, SW Japan. Journal of Structural Geology 14, 271–280.

Wallis, S.R., 1995. Vorticity analysis and recognition of ductile extension in the Sanbagawa belt, SW Japan. Journal of Structural Geology 17, 1077–1093.

Wallis, S.R., Platt, J.P., Knott, S.D., 1993. Recognition of synconvergence extension in accretionary wedges with examples from the Calabrian Arc and the Eastern Alps. American Journal of Science 293, 463–495.

Wells, M.L., 1997. Alternating contraction and extension in the hinterlands of orogenic belts: an example from the Raft River Mountains, Utah. Geological Society of America Bulletin 109, 107–126.

Wells, M.L., 2001. Rheological control on the initial geometry of the Raft River detachment fault and shear zone, western United States. Tectonics 20, 435–457.

Wells, M.L., Snee, L.W., Blythe, A.E., 2000. Dating of major normal fault systems using thermochronology: an example from the Raft River detachment, Basin and Range, western United States. Journal of Geophysical Research 105, 16303–16327.

Wenk, H.R., Canova, G., Molinari, A., Kocks, U.F., 1989. Visco-elastic modeling of texture development in quartzite. Journal of Geophysical Research 94, 17,895–17,906.

Wernicke, B., Axen, G.J., 1988. On the role of isostasy in the evolution of normal fault systems. Geology 16, 848–851.

White, S.H., 1976. The effects of strain on the microstructures, fabrics and deformation mechanisms in quartzites. Philosophical Transactions of the Royal Society of London 283, 69–86.

Whitney, D.L., Teyssier, C., Vanderhaeghe, O., 2004. Gneiss domes and crustal flow. In: Whitney, D.L., Teyssier, C., Siddoway, C.S. (Eds.), Gneiss Domes and Orogeny. Geological Society of America, Special Paper, vol. 380, pp. 15–33.